Acta Oceanologica Sinica, Vol. 21, No. 2, pp. 227~261, 2002. ISSN 0253-505X
Published by China Ocean Press.

The South China Sea thermohaline structure and circulation*

Peter C. Chu[1], Binbing Ma[1], Yuchun Chen[2]

(*Received March* 21, 2002; *accepted April* 10, 2002)

Abstract —— In this study, we used the Navy's Master Oceanographic Observation Data Set (MOODS), consisting of 116 019 temperature and 9 617 salinity profiles, during 1968~1984 to investigate the temporal and spatial variabilities of South China Sea thermohaline structures and circulation. For temperature, profiles were binned into 204 monthly data sets from 1968 to 1984 (17 years). For salinity, profiles were binned into 12 climatological monthly data sets due to the data paucity. A two-scale optimal interpolation method was used to establish a three-dimensional monthly-varying gridded data set from MOODS, covering the area of 5°~25°N and 105°~125°E and the depth from the surface to 400 m. After the gridded data set had been established, both composite analysis and the Empirical Orthogonal Function (EOF) analysis (for temperature only) were used to identify the major thermohaline fratures including annual mean, monthly anomalies, and interannual thermal variabilities. The inverted monthly circulation pattern using the P − vector method is also discussed.

Key words The South China Sea, thermohaline structure, circulation

INTRODUCTION

The South China Sea (SCS), the largest marginal sea in the West Pacific Ocean, is separated from adjacent oceans by a chian of islands. It contains the broad shallow Sunda Shelf on the south, a shelf extending from the Gulf of Tonkin to the Taiwan Strait on the north, A deep sea basin in the center, and dangerous ground with numerous reef islands over the southeast (see Fig.1). It has a hottom topography that makes it a unique semi-enclosed ocean basin overlaid by a pronounced monsoon surface wind. Extensive continental shelves (less than 100 m deep) are found on the western and southern parts, while steep slopes with almost no shelves are found in the eastern part of SCS. The deepest water is confined to a bowel-type

* This study was funded by the Office of Naval Research NOMP Program, the Naval Oceanographic Office, and the Naval Postgraduate School.

1. Naval Postgraduate School, Monterey, California, USA
2. Cold and Arid Regions Environmental and Engineering Research Institute Chinese Academy of Sciences, Lanzhou, China

Fig. 1. Geography and isobaths showing the bottom topography of the South China Sea.

trench and the maximum depth is approximately 4 700 m.

Based on limited data sets, studies show that surface eddies in the SCS are predominantly cyclonic in winter and spring and anti-cyclonic in summer, with sizes ranging from small to meso-scale (Wyrtki, 1961; Huang *et al*., 1994). Both cold and warm eddies exist in the SCS. Dale (1956) and Uda and Nakao (1972) reported a cold eddy off the central Vietnamese Coast in summer, and Nitani (1970) found a cold eddy located to the northwest of Luzon. Reports from the South China Sea Institrte of Oceanology (SCSIO, 1985) indicate that in the in the central SCS a warm-core eddy appears in summer and winter, but it is closer to Vietnam in summer at the surface. In addition, a cold-core eddy was detected in the central SCS from the 29th December 1993 to 5th January 1994 according to analysis of the TOPEX/POSEIDON data (Soong *et al*., 1995).

Recently, Chu *et al*. (1997a) and Chu and Chang (1997) identified a central SCS sur-

face warm-core eddy in Mid-May from a more complete historical data set — the U. S. Navy's Master Observational Oceanographic Data Set (MOODS). From the composite analysis of the U. S. National Centers for Environmental Prediction (NCEP) monthly SST fields (1982～1994), Chu *et al*. (1997b) found that during the spring-to-summer monsoon transition (march to May) a warm anomaly (greater than 1.8℃) is formed in the central SCS at 122°～119°30′E, 15°～19°30′N. This warm eddy appears in the central SCS (west of the Luzon Island) during the late spring season and strengthens until the onset of the summer monsoon (mid-May) and then weakens and disappears at the end of May. Although its size and intensity varies, the SCS warm pool releases large moisture and heat fluxes into the atmosphere and in turn affects the monsoon circulation. Most of the existing studies on the seasonal eddy variability were based on the surface data (e. g., Chu *et al*., 1997a, b) or on limited data (e. g., Chu *et al*., 1998b; Chu and Fan, 2001). What is the three-dimensional SCS thermohaline structure and its seasonal and interannual variabilities? We will investigate these questions in this study.

The outline of this paper is as follows: Section 2 describes the U. S. Navy's Master Oceanographic Observation Data Set (MOODS) and the establishment of gridded data. Section 3 depicts the composite analysis to obtain temperature and salinity seasonal variations. Section 4 describes the EOF method to obtain nonseasonal thermal variabilities. Section 5 present the SCS circulation using the q – vector inverse method major current systems and seasonal variation, and Section 6 presents our conclusions.

MASTER OCEANOGRAPHIC OBSERVATION DATA SET (MOODS)

T, *S profiles*

We use the Navy's Master Observational Oceanographic Data Set (MOODS) for the study. The MOODS is a compilation of observed ocean data worldwide consisting of (a) temperature-only profiles; (b) both temperature and salinity profiles; (c) soundspeed profiles; and (d) surface temperature (drifting buoy). These measurements are, in gengeal, irregular in time and space. The data are from the early nineteenth century to the present and include 116 019 temperature profiles (see Fig.2a) and 9 617 salinity profiles (see Fig.2b) between 1964 to 1984. In this study, we analyze the temperature profiles obtained during 1986～1984 from a variety of instruments. Our study domain includes the area 5°N to 25°N and 105°E to 125°E.

The primary editing procedures included removal of profiles with obviously erroneous location profiles with large spikes, and profiles displaying features that do not match the characteristics of surrounding profiles. In shallow water, this procedure can be partially automated, but it also involves subjective interpretation because of the under sampling of MOODS, compared to the spatial and temporal variability of the ocean. The temporal and spatial distribution of the MOODS data are irregular (Chu *et al*., 1997a).

Furthermore, vertical resolution and data quality are also highly variable depending much on instrument type and sampling expertise. Temporal and spatial irregularities along with the data resolution and quality problems must be carefully weighed in order to avoid mathematically-induced variability.

Establishment of monthly gridded data

We binned seventeen years' temperature profiles from 1968 to 1984 into monthly data for an individual year which produced 204 temperature data sets. For the salinity profiles, we bin-

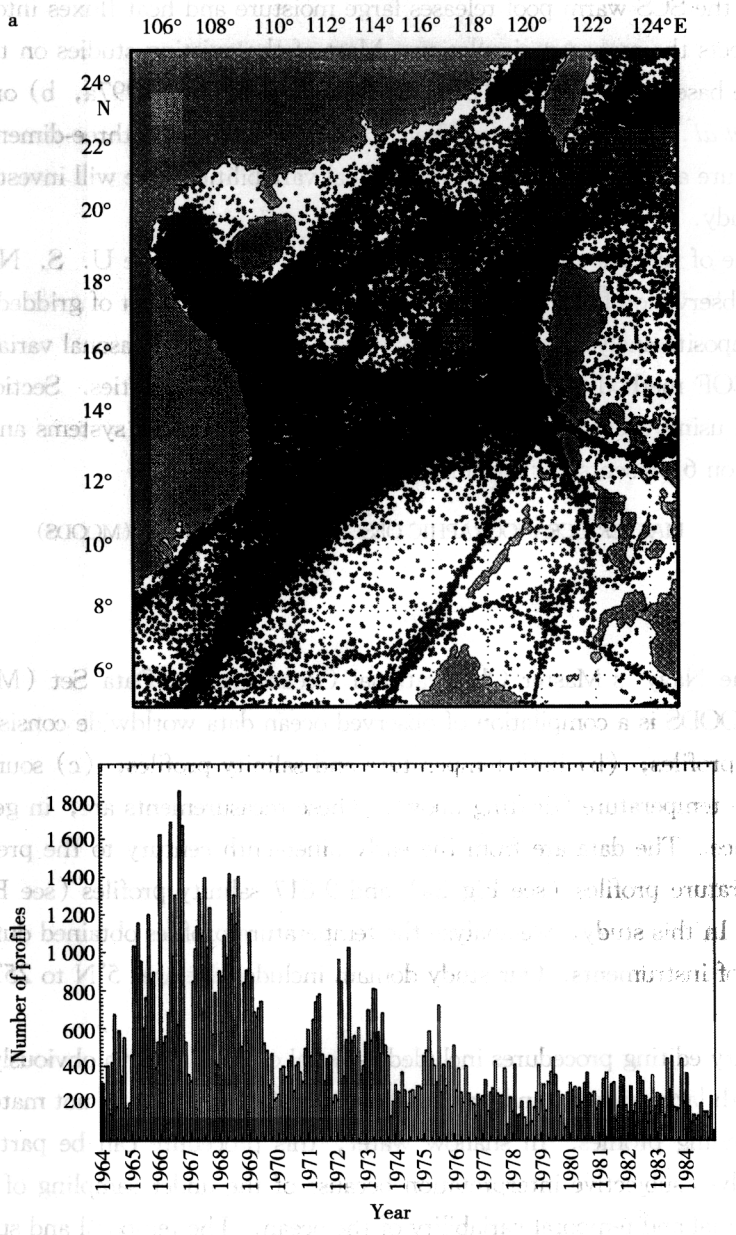

Fig. 2a

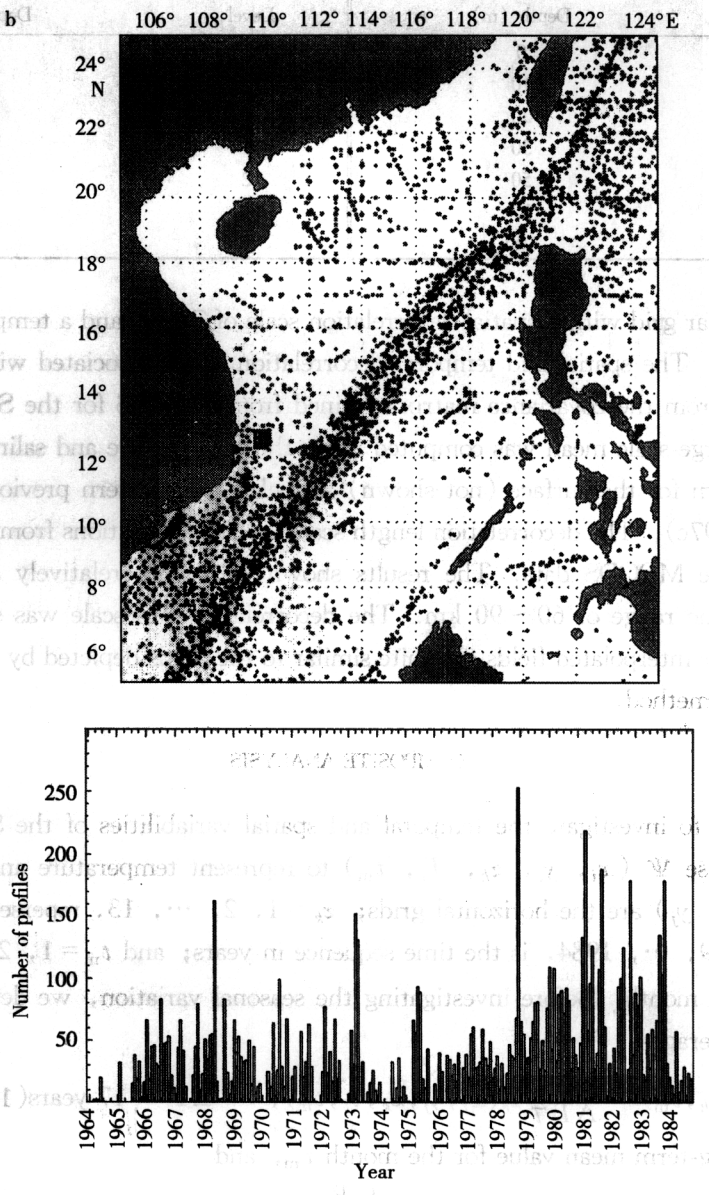

Fig. 2. Spatial and temporal disributions of MOODS stations during 1964～1984 for this study: (a) temperature and (b) salinity.

ned profiles into monthly climatology data bins which produced 12 mean monthly salinity data sets. We used a two-scale optimal interpolation (OI) scheme (Gandin, 1965; Lozano *et al.*, 1996) to map the MOODS observations to a $0.5° \times 1°$ grid (finer resolution in the zonal direction) at 13 levels (see Table 1) and to establish a monthly synoptic temperature data set from 1968 to 1984 (total 204 fields) and a monthly climatology salinity data set (total 12 fields). The large-scale OI was used to estimate the background mean with a decorrelation scale of 450 km. The mesoscale OI was used to map the observational anomaly from the background mean

Table 1. Distribution of vertical levels

Level	Depth (m)	Level	Depth (m)
1	0	8	125
2	10	9	150
3	20	10	200
4	30	11	250
5	50	12	300
6	75	13	400
7	100		

field into a regular grid with a spatial decorrelation scale of 75 km and a temporal decorrelation scale of 10 days. The spatial and temporal decorrelation scales associated with the mean field were estimated from the covariance matrix obtained from MOODS for the SCS (Chu *et al.*, 1997c). The large-scale mean was computed using the temperature and salinity profiles. The large-scale pattern for the surface (not shown) resembles the pattern previously estimated by Chu *et al.* (1997c). The decorrelation length scale for the fluctuations from the mean was estimated from the MOODS data. The results shown below are relatively insensitive to the length scale in the range of 60～90 km. The decorrelation timescale was selected to ensure synopticity. Our interpolated fields are quite similar to the fields depicted by Ma (1998) using the cubic spline method.

COMPOSITE ANALYSIS

Our goal is to investigate the temporal and spatial variabilities of the SCS thermohaline structure. We use $\Psi\ (x_i,\ y_i,\ z_k,\ T_l,\ t_m)$ to represent temperature and salinity gridded data where $(x_i,\ y_j)$ are the horizontal grids; $z_k = 1,\ 2,\ \cdots,\ 13$, repersent vertical levels; $T_l = 1968,\ 1969,\ \cdots,\ 1984$, is the time sequence in years; and $t_m = 1,\ 2,\ \cdots,\ 12$, is the time sequence in month. Before investigating the seasonal variation, we define the following two temporal averages:

$$\overline{\Psi}(x_i, y_j, z_k, t_m) \equiv \frac{1}{\Delta T}\sum_l \Psi(x_i, y_j, z_k, \tau_l, t_m), \qquad \Delta T \equiv 17 \text{ years}(1968 \sim 1984) \quad (1)$$

which is the long-term mean value for the month t_m, and

$$\overline{\overline{\Psi}}(x_i, y_j, z_k) \equiv \frac{1}{12}\sum_{m=1}^{12} \overline{\Psi}(x_i, y_j, z_k, t_m), \quad (2)$$

which is the annual mean.

The monthly data $\Psi\ (x_i,\ y_j,\ z_k,\ \tau_l,\ t_m)$ relative to its annual mean are expressed as follows:

$$\hat{\Psi}(x_i, y_j, z_k, \tau_l, t_m) = \Psi(x_i, y_j, z_k, \tau_l, t_m) - \overline{\overline{\Psi}}(x_i, y_j, z_k). \quad (3)$$

Annual mean fields

Temperature.

The annual mean (1968～1984) temperature $\overline{\overline{T}}$ field over the SCS shows the pattern of

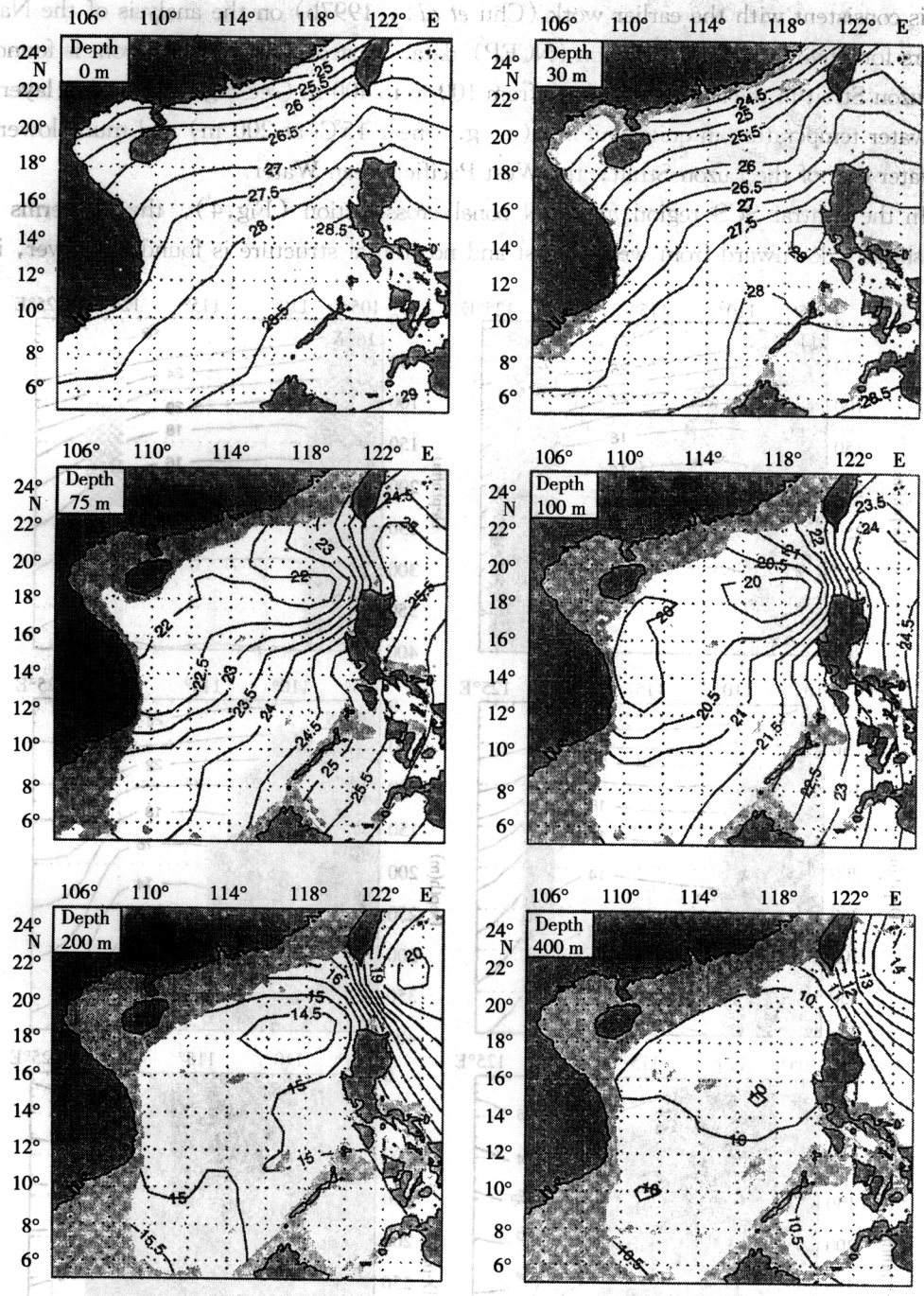

Fig. 3. Annual mean temperature (℃) field at: surface, 30 m, 75 m, 100 m, 200 m and 400 m.

northeast-southwest oriented isotherms at the upper layer from the surface to 75 m depth (Fig.3). The annual surface mean temperature has a rather weak horizontal temperature gradient, decreasing from 28.5℃ near the Borneo coast to 25℃ near the southeast China coast.

This is consistent with the earlier work (Chu *et al*., 1997b) on the analysis of the National Centers for Environmental Prediction (NCEP) data. A strong temperature front is found near the Luzon Strait in the sub-surface layer from 100 m to 400 m (see Fig.3). In that layer, the SCS water temperature in quite uniform (e. g., near 15℃ at 200 m) and much lower than the water east of the Luzon Strait, the West Pacific Ocean Water.

In the central SCS region at 16° N zonal cross-section (Fig.4), the isotherms of $\overline{\overline{T}}$ bend slightly downward from west to east and no frontal structure is found, however, in the

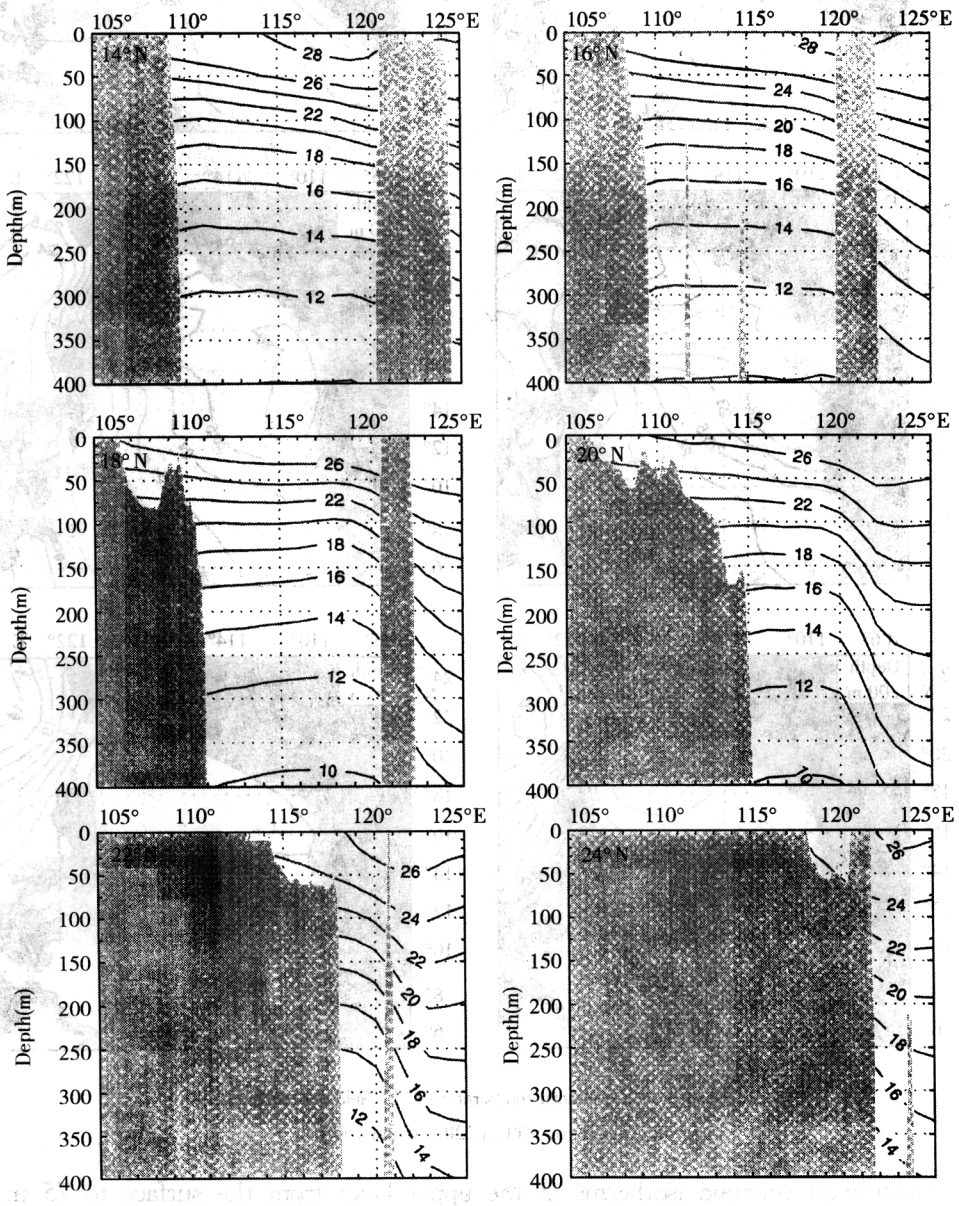

Fig. 4. Zonal cross-sections of annual mean temperature (℃): 14°N, 16°N, 18°N, 20°N, 22°N and 24°N.

northern SCS region at 20°N zonal cross-scetion, the isotherms of $\overline{\overline{T}}$ show a strong frontal structure near 120° to 125°E (see Fig.4), which may suggest two distinguished water masses, the SCS water mass (both surface and under-surface) and the West Pacific Ocean water mass. The front between the two water masses strengthens from the surface to 400 m in depth.

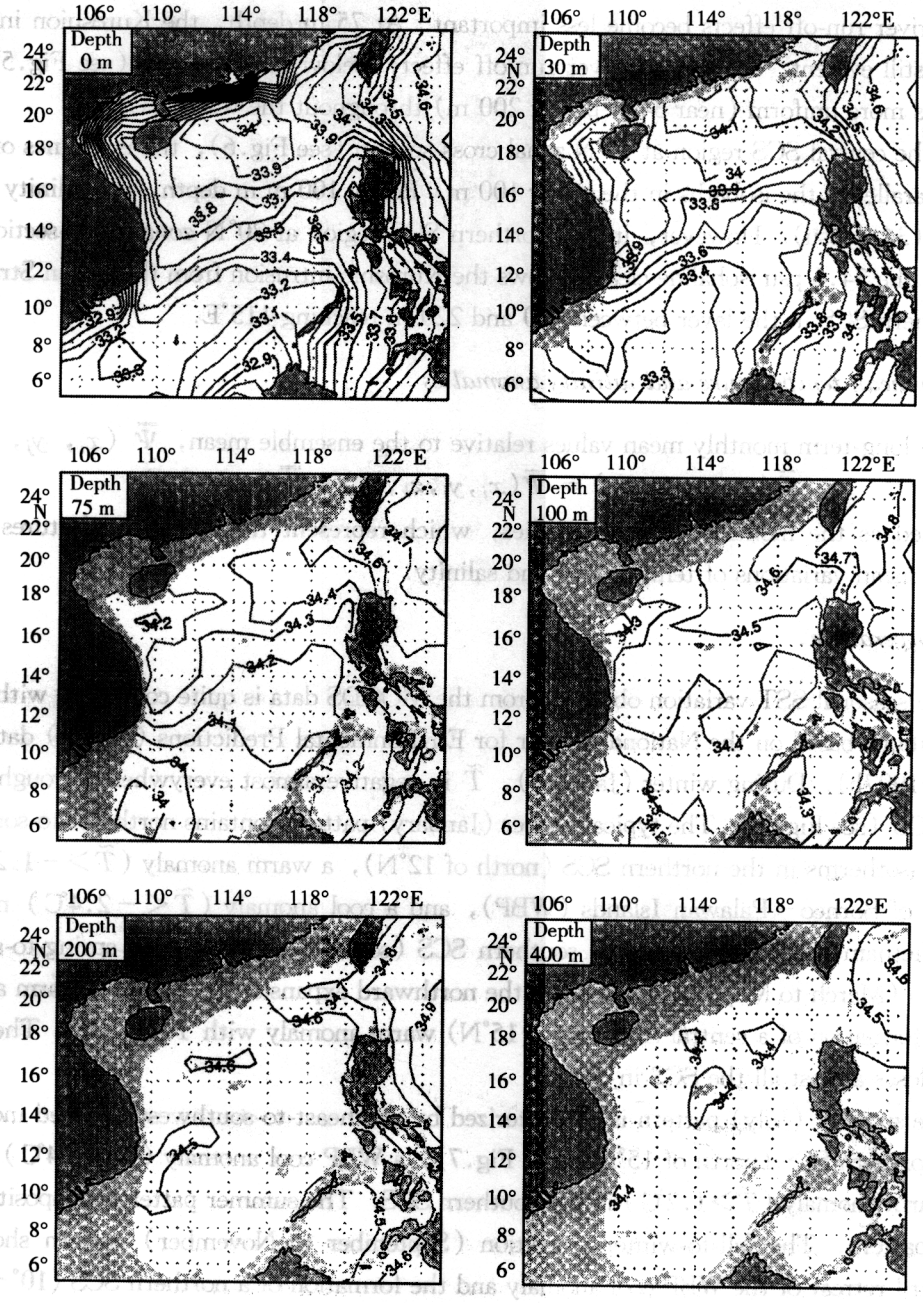

Fig. 5. Annual mean salinity (psu) field at: surface, 30 m, 75 m, 100 m, 200 m and 400 m.

Salinity.

The annual mean salinity $\bar{S}$ field shows more complexity than temperature. In the upper layer (see Fig.5), a large amount of freshwater enters the SCS from the Zhujiang (Pearl) River in the northwest and from the Mekong River in the southwest. The Kuroshio brings the salty water through the Luzon Strait into the north SCS and forms a salty tongue (34 psu) stretching into the southeast China coast. As the depth increases both the Kuroshio intrusion and the river run-off effects become less important. At 75 m depth, the Kuroshion intrusion effect is still evident, but not the river run-off effect, Below 200 m depth (see Fig.5), the salinity is more uniform (near 34.6 psu at 200 m) throughout the whole SCS.

In the central SCS region at 15°N zonal cross-section (see Fig.6), the isohalines of $\bar{S}$ are almost parallel to the isobaths in the upper 100 m. Below 100 m in depth, the salinity is very uniform (34.4 psu). However, in the northern SCS region at 20°N zonal cross-section (see Fig.6), the 34.6 psu isohaline clearly shows the Kuroshio intrusion from the Luzon Strait into the northern SCS in the layer between 100 and 220 m reaching 115°E.

Monthly mean temperature and salinity anomalies

The long-term monthly mean values relative to the ensemble mean, $\bar{\bar{\Psi}}(x_i, y_j, z_k)$,

$$\tilde{\Psi}(x_i, y_j, z_k, t_m) = \bar{\Psi}(x_i, y_j, z_k, t_m) - \bar{\bar{\Psi}}(x_i, y_j, z_k) \tag{4}$$

are defined as the monthly mean anomalies, which represent the composite features of the monthly mean variations of temperature and salinity.

Temperature.

The seasonal SST variation obtained from the MOODS data is quite consistent with earlier investigations based on the National Center for Environmental Predictions (NCEP) data (Chu *et al*., 1997b). During winter (January), $\tilde{T}$ is negative almost everywhere throughout the whole SCS (see Fig.7). The typical winter (January) pattern contains northeast-to-southwest oriented isotherms in the northern SCS (north of 12°N), a warm anomaly ($\tilde{T} > -1.2$℃) in the west of Borneo－Palawan Islands (WBP), and a cool anomaly ($\tilde{T} < -2.4$℃) near the South Vietnam Coast (SVC) in the southern SCS (south of 12°N). The spring-to-summer transition (March to May) pattern shows the northward expansion of the WBP warm anomaly and the formation of a central SCS (10°～15°N) warm anomaly with $\tilde{T} > 0.6$℃. The isoline 1℃ encloses almost all the SCS in May.

The summer (July) pattern is characterized by northeast-to-southwest oriented inotherms in the northern SCS (north of 15°N) (see Fig.7), a WBP cool anomaly ($\tilde{T} < 0.4$℃), and a SVC warm anomaly ($\tilde{T} > 1.2$℃) in the southern SCS. The summer pattern is opposite to the winter pattern. The fall-to-winter transition (September to November) pattern shows the southward retreat of the WBP cool anomaly and the formation of a northern SCS (10°～15°N) cool anomaly possibly caused by the onset of northeast winter monsoon.

We chose 200 m depth as the intermediate level. At 200 m depth, the seasonal variation

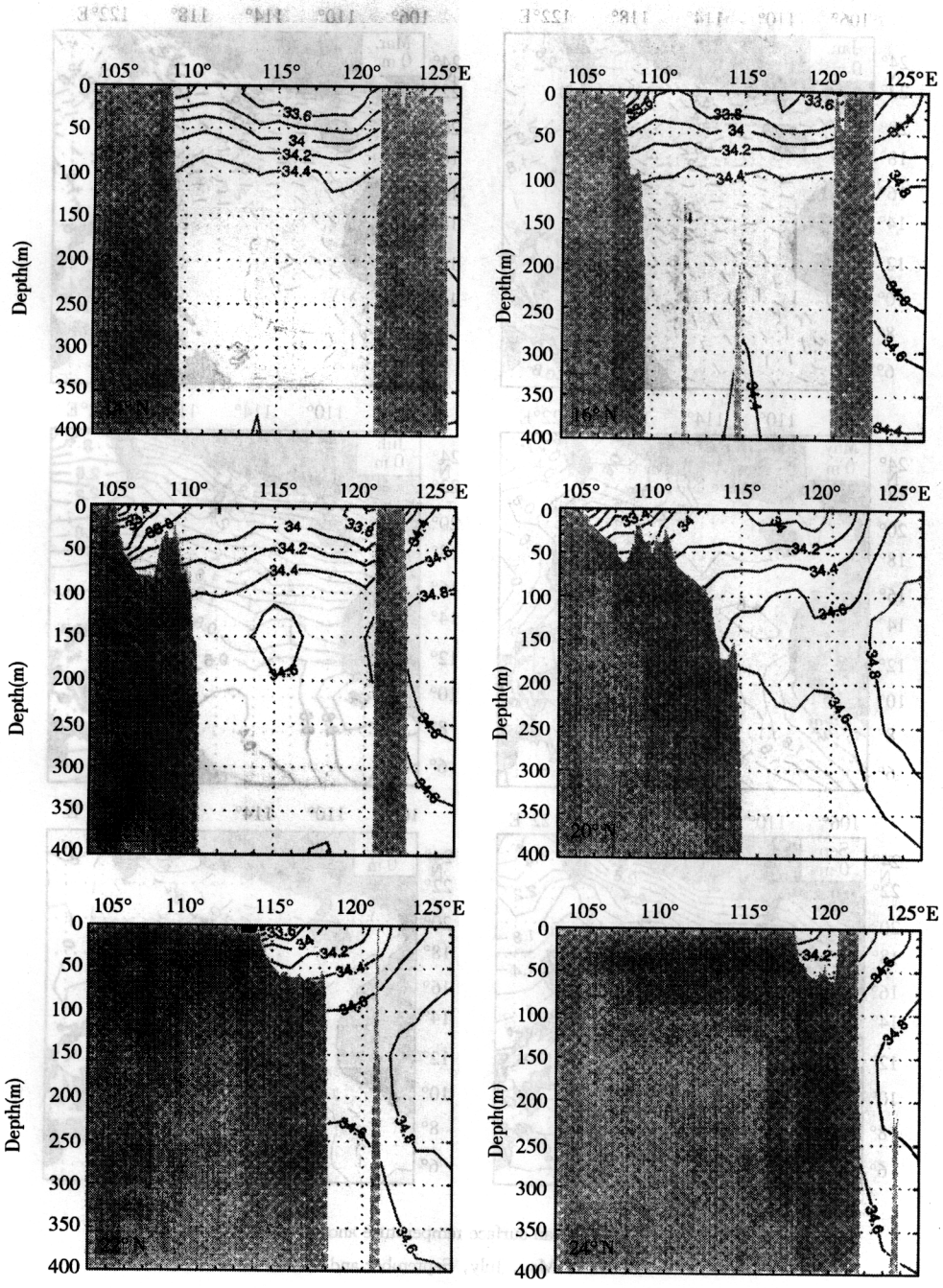

Fig. 6. Zonal cross-sections of annual mean salinity: 14°N, 16°N, 18°N, 20°N, 22°N and 24°N.

of temperature is featured by a basin-wide cool pool ($\tilde{T}<-0.8$℃), a strong SCC warm pool ($\tilde{T}>0.8$℃,), and a weak WBP warm pool ($\tilde{T}>0.2$℃) during the winter (see Fig.8) and a basin-wide warm pool ($\tilde{T}>0.4$℃), and a weak SVC cool pool ($\tilde{T}<0$℃) during the summer (see Fig.8). The west Luzon coast (WLC) winter cool eddy ($\tilde{T}<-1.0$℃) and summer

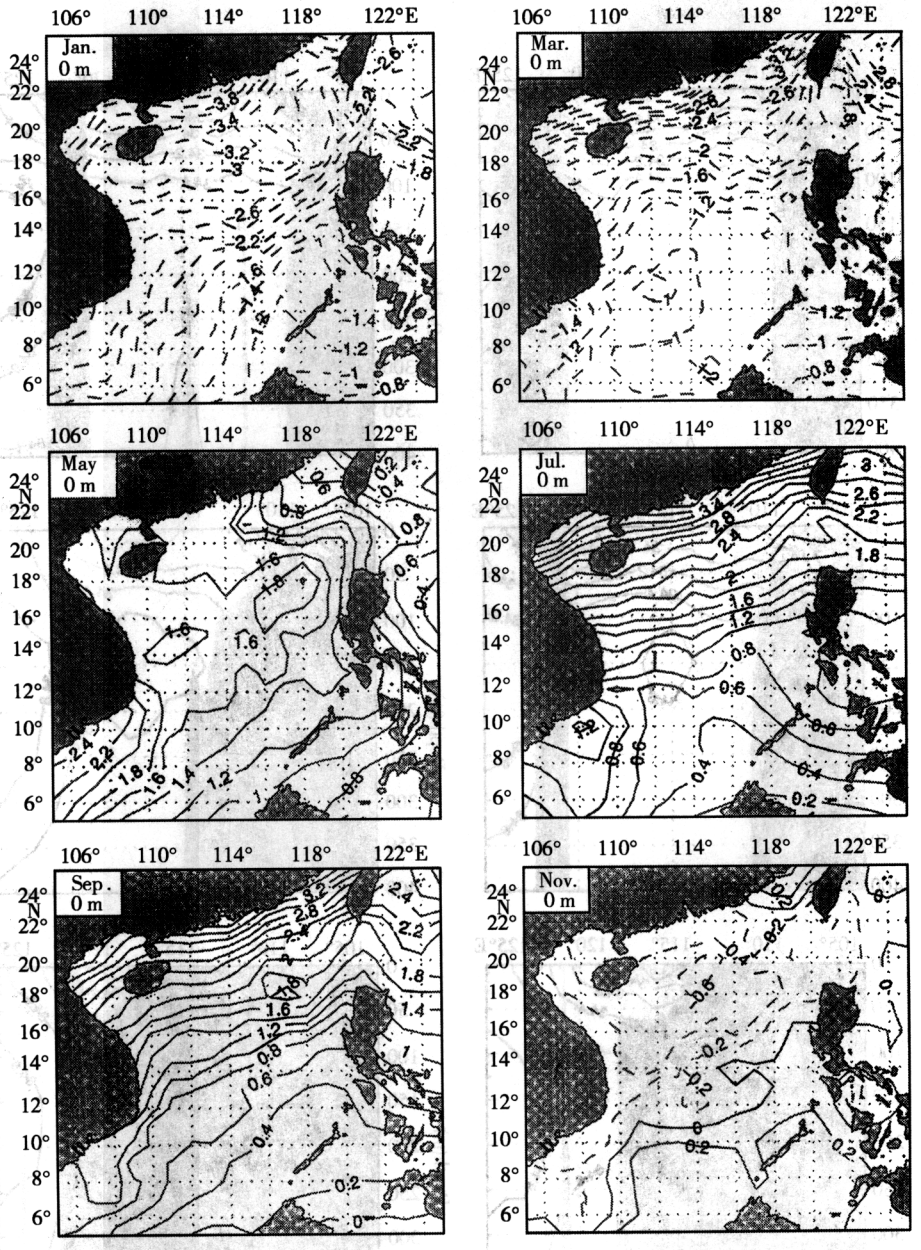

Fig. 7. Monthly mean surface temperature anomalies (℃) in: January, March, May, July, September and November.

warm eddy ($\tilde{T}>0.8$℃) are still quite evident at that depth. A weak WLC warm eddy ($\tilde{T}>0.2$℃) occurs and expands toward the west in spring (see Fig.8), gradually occupies the whole SCS basin, and turns to the summer pattern in July (see Fig.8). In autumn, the weak SVC cool disappears. A weak cold pool stretches from the east of Taiwan toward the southwest, gradually occupies the whole SCS basin, and turns to winter pattern in January. Below 300 m depth, there is no significant seasonal variability.

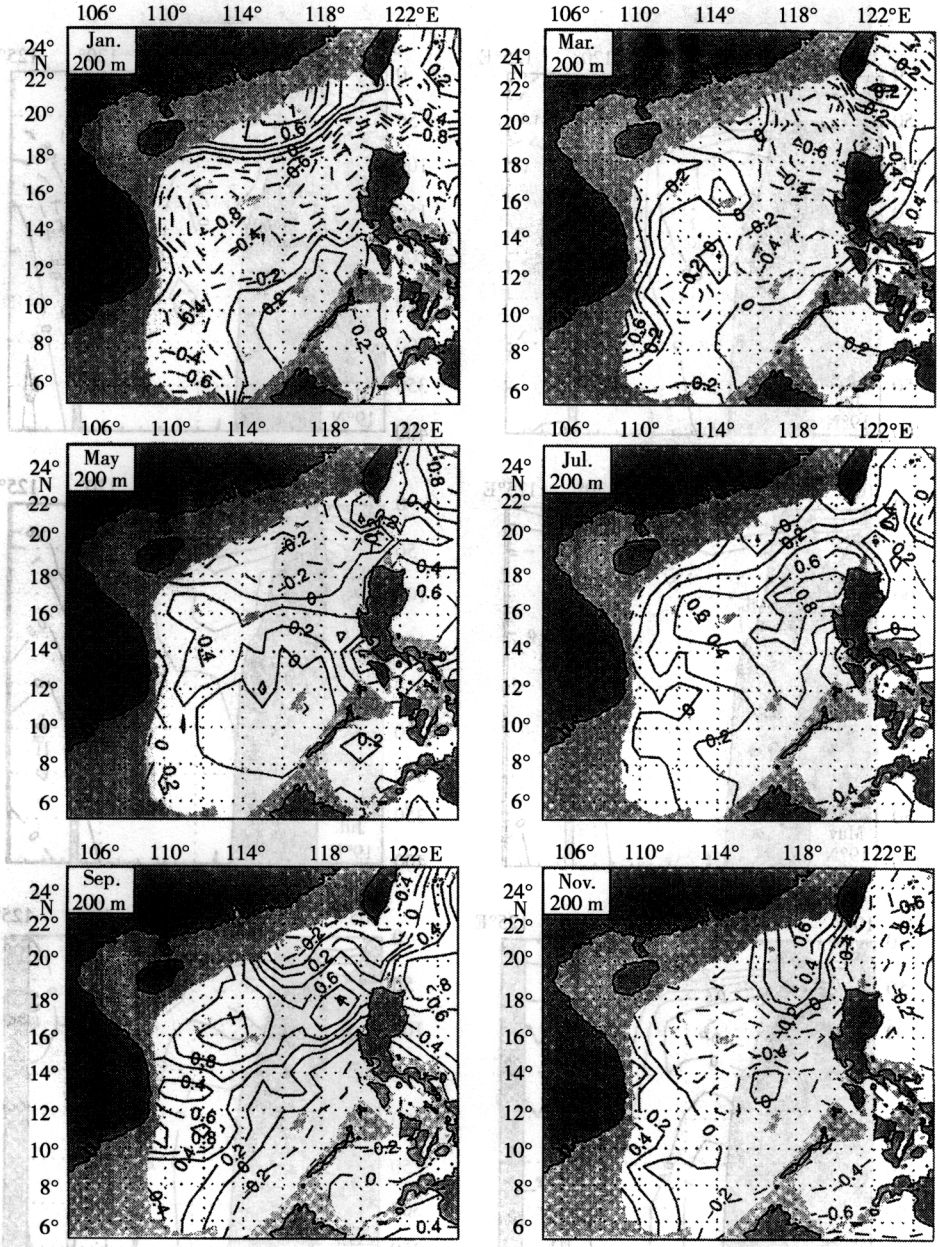

Fig. 8. Monthly mean temperature anomalies (℃) at 200 m depth in: January, March, May, July, September and November.

The zonal cross-section at 19°N of the $\tilde{T}$ field, shows the vwrtical structure of the WLC cool eddy in winter (see Fig.9), and the vertical structure of the WLC warm eddy in summer (see Fig.9). Both WLC winter cool and summer warm eddies reach 250 m depth. The winter cool-core ($\tilde{T}<-3$℃) and the summer warm - core ($\tilde{T}>2.5$℃) are located between 50 m to 100 m depth.

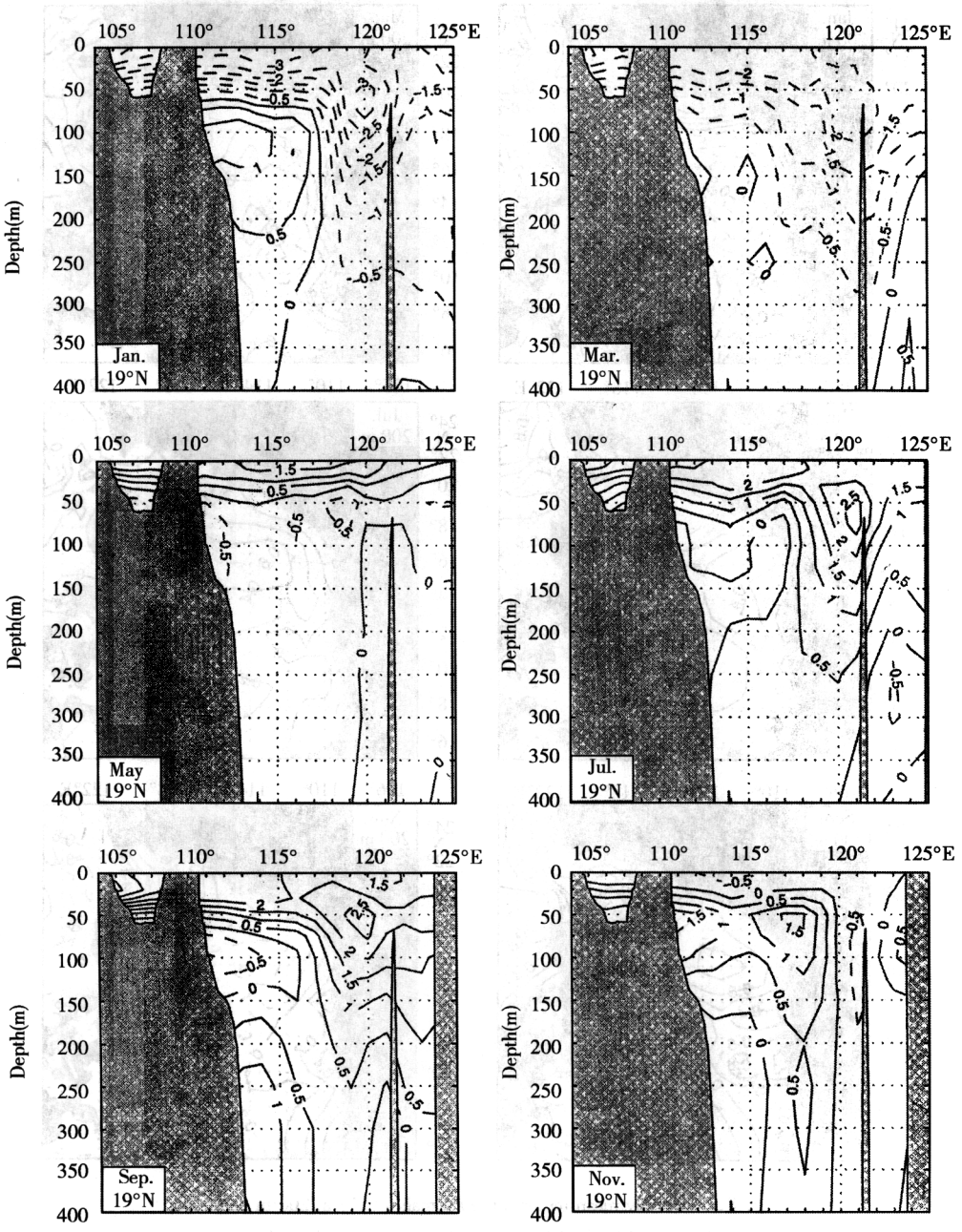

Fig. 9. Zonal cross-sections of monthly mean temperature anomalies (℃) at 19°N in: January, March, May, July, September and November.

Salinity.

The seasonal salinity variation $\tilde{S}$ is evident only in the layer above 200 m in depth. Below this depth, the seasonal variability is very weak.

Surface salinity experiences a strong seasonal variation. During winter (January), $\tilde{S}$ is positive almost everywhere throughout the whole SCS except the SVS and the Gulf of Tonkin (Fig.10). A salty tongue with $\tilde{S}>0.4$ psu stretches from the Luzon Strait to the continental shelf along the southeast China coast, representing a strong Kuroshio intrusion. Another weak fresh pool with $\tilde{S}<-0.2$ psu is found to the west of Luzon Island. During summer (July), a salty tongue with $\tilde{S}$ around 0.4 psu stretches from the Vietnam coast to 118°E between 10°~

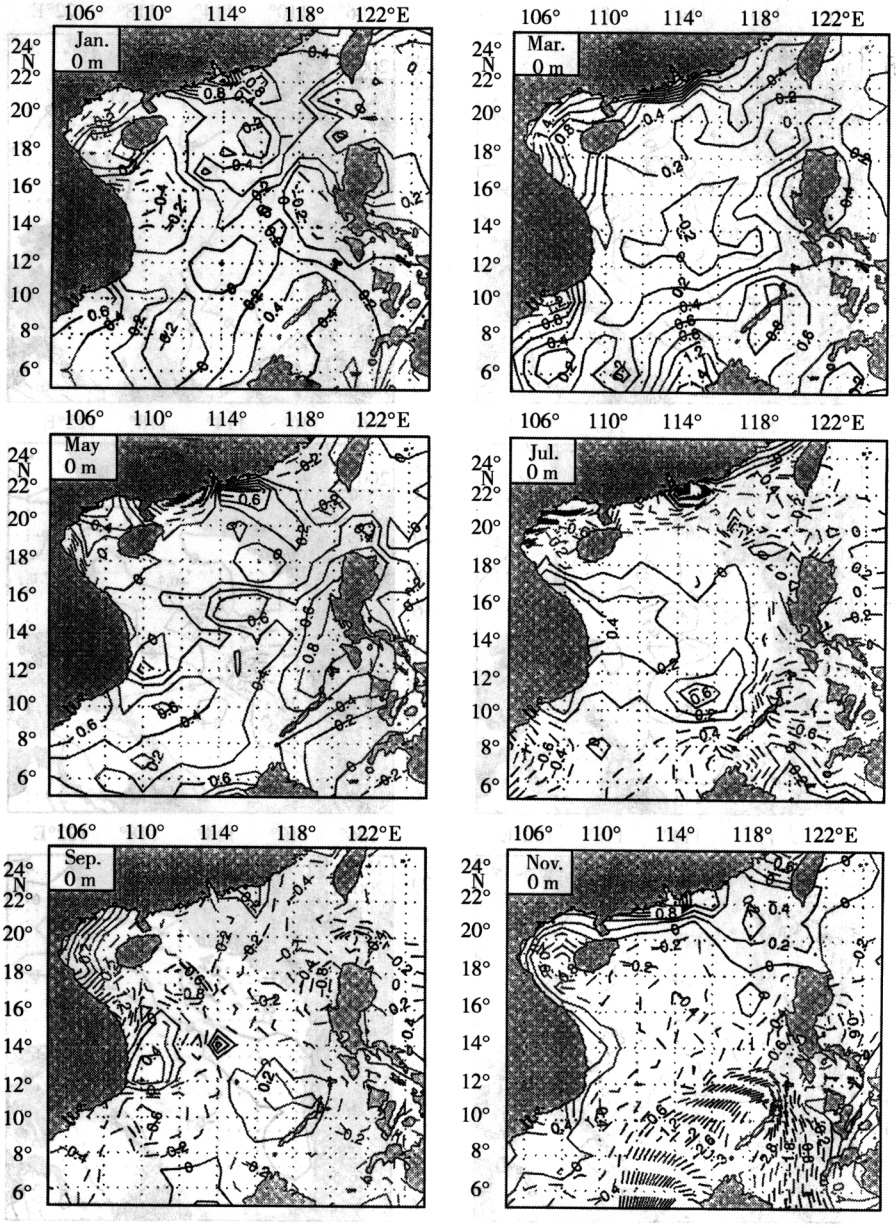

Fig. 10. Monthly mean surface salinity anomalies (psu): January, March, May, July, September and November.

17°N, occupying the central SCS (see Fig.10). Everywhere else is occupied by negative $\tilde{S}$. A strong fresh tongue occupies the continental shelf along the southeast China coast and the Gulf of Tonkin.

At 200 m depth, the seasonal variation of $\tilde{S}$ is also evident. In the winter (Fig.11), positive $\tilde{S}$ with a maximum value of 0.3 psu occupies the most area of the SCS, except the southwest corner ner the Mekong River, where $\tilde{S}$ is negative (-0.4 pus). In the summer

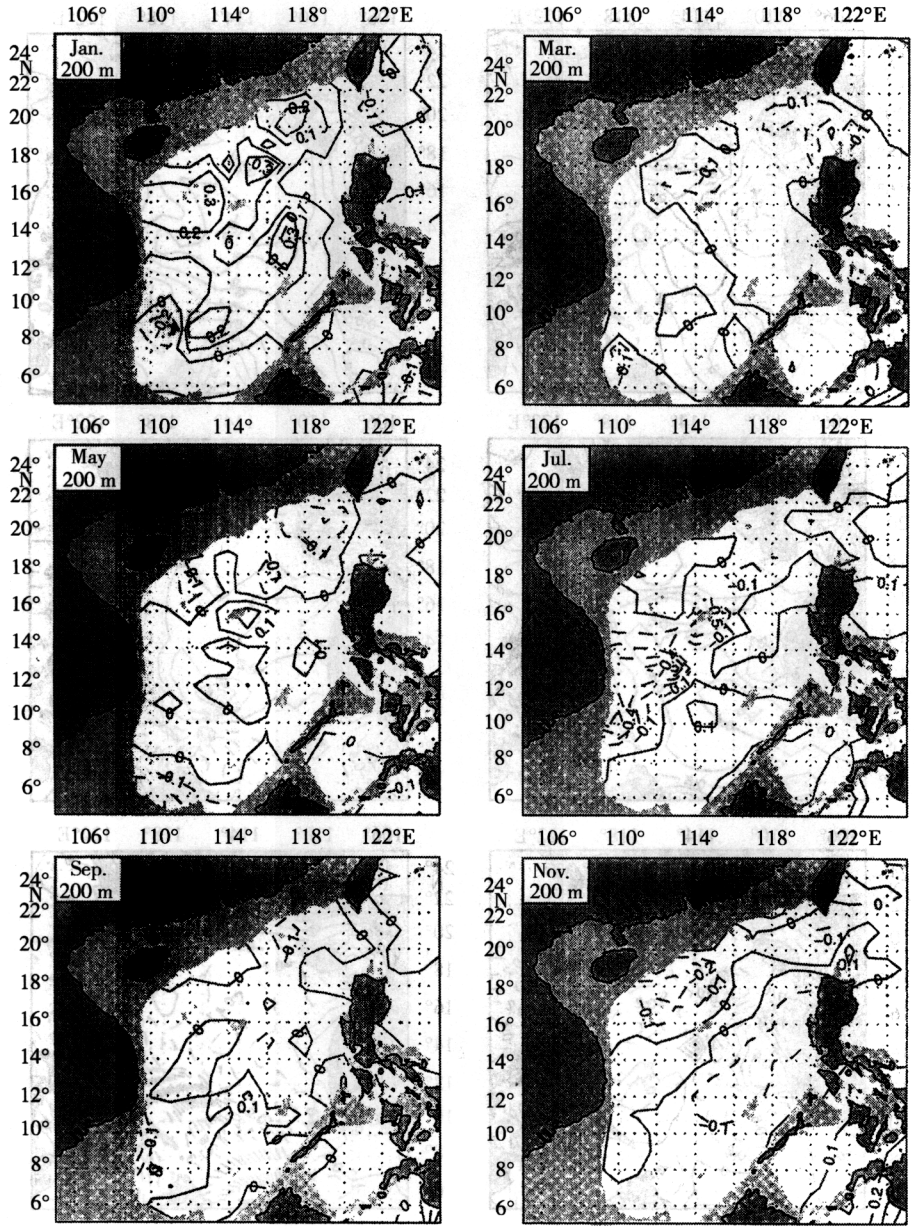

Fig. 11. Monthly mean salinity anomalies (psu) at 200 m depth: January, March, May, July, September and November.

(see Fig.11), a narrow fresh tongue with a minimum value of −0.4 psu stretches northeastward from the southwest corner near the Mekong River to 20°N (see Fig.11).

The zonal cross-section at 19°N of the $\tilde{S}$ field, shows the vertical structure of the WLC high salinity anomaly ($\tilde{S}>0.4$ psu) in winter (see Fig.12) and low salinity anomaly ($\tilde{S}<$

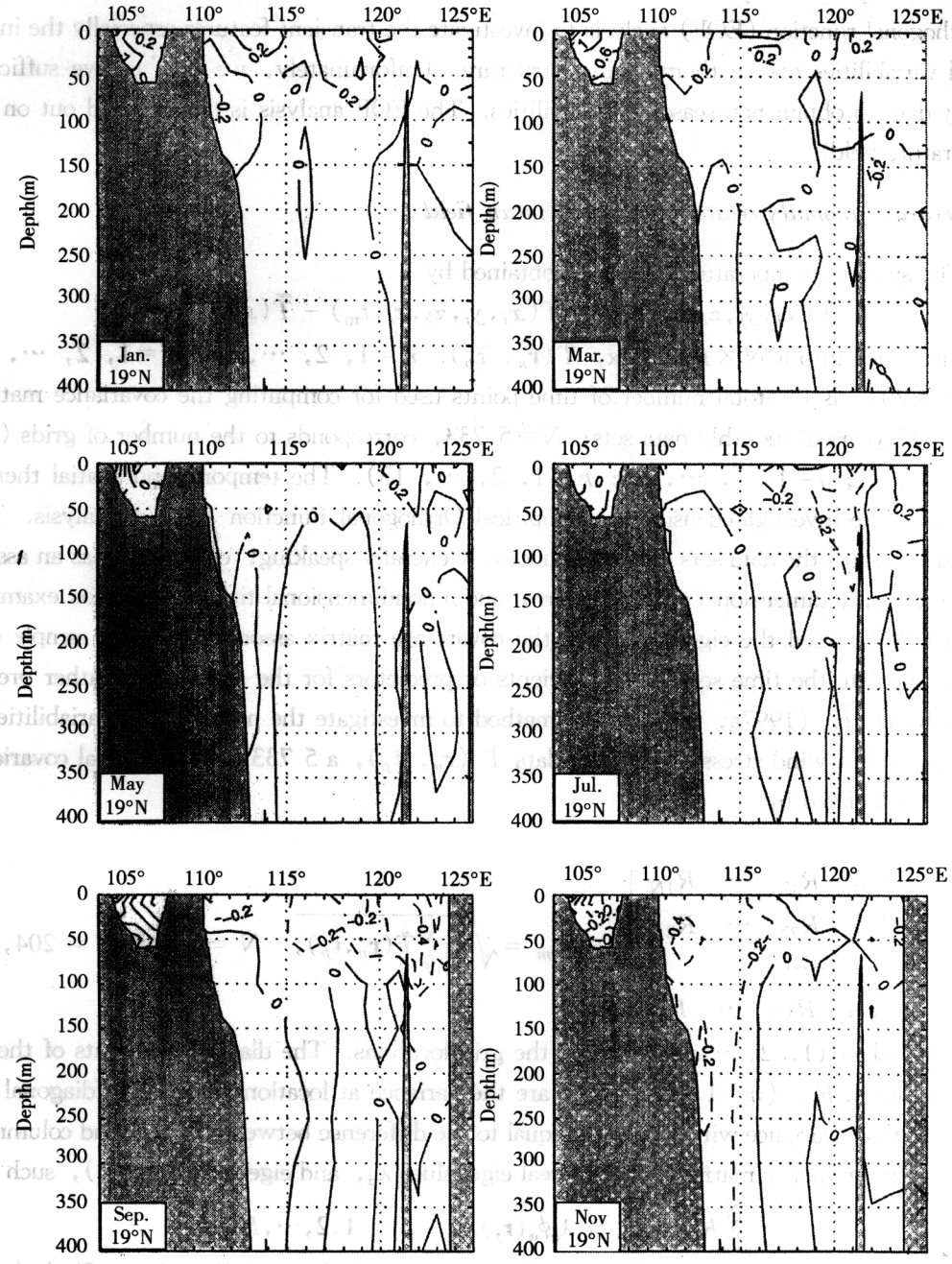

Fig. 12. Zonal cross-sections of monthly mean salinity anomalies (psu) at 19°N: January, March, May, July, September and November.

−0.2 psu) in summer (see Fig.12). Both WLC high/low salinity anomalies are located at a depth between 50 m to 100 m.

EMPIRICAL ORTHOGONAL FUNCTION (EOF) ANALYSIS

The composite analysis shows the mean seasonal T, S variabilities. Next we use empirical orthogonal runction (EOF) analysis to investigate the transient features especially the interannual variabilities of the thermohaline structure. Unfortunately, we don't have sufficient salinity data to obtain non-seasonal variabilities. The EOF analysis is only carried out on the temperature field.

Temperature anomaly relative to annual mean field

The synoptic temperature anomalies obtained by

$$\hat{T}(x_i, y_j, z_k, \tau_l, t_m) = T(x_i, y_j, z_k, \tau_l, t_m) - \bar{\bar{T}}(x_i, y_j, z_k) \tag{5}$$

are re-arranged into a $N \times P$ matrix, $\hat{T}(\mathbf{r}_n, \tilde{t}_p)$. $n = 1, 2, \cdots$, and $p = 1, 2, \cdots, P$. Here $P = 204$, is the total number of time points used for computing the covariance matrix, that is, 17 years of monthly data sets; $N = 5\ 733$, corresponds to the number of grids ($i = 1, 2, \cdots, 21$; $j = 1, 2, \cdots, 21$; $k = 1, 2, \cdots, 13$). The temporal and spatial thermal variabilities are investigated using the Empirical Orthogonal Function (EOF) analysis. This method separates the data sets into eigenmodes. Generally speaking, each mode has an associated variance, a dimensional spatial pattern, and a nondimensional time series. Fox example, Lorenz (1965) used the eigenvectors of the covariance matrix associated with a sample data field to calculate the time series of coefficients or predictors for the statistical weather prediction. Chu *et al*. (1997a, b) used this method to investigate the non-seasonal variabilities of SST and surface wind stress. From our data $\hat{T}$ $(\mathbf{r}_n, \tilde{t}_p)$, a 5 733×5 733 spatial covariance matrix is calculated by

$$R = \begin{bmatrix} R_{11} & R_{12} & \cdots & R_{1N} \\ R_{21} & R_{22} & \cdots & R_{2N} \\ & \cdots\cdots & & \\ R_{N1} & R_{N2} & \cdots & R_{NN} \end{bmatrix}, \quad R_{nm} = \sqrt{\frac{1}{P}\sum_p \hat{T}(\mathbf{r}_n, \tilde{t}_p)}, \quad N = 5\ 733, P = 204, \tag{6}$$

where n and m $(1, 2, \cdots, N)$ denote the grid locations. The diagonal elements of the covariance matrix R_{nn} $(n = 1, 2, \cdots N)$ are the variance at location $\mathbf{r}_n$. The offdiagonal elements are the covariance with spatial lag equal to the difference between the row and column indices. This symmetric matrix has its N real eigenalues λ_α, and eigenvectors$\phi_\alpha(\mathbf{r}_j)$, such that

$$\sum_{j=1}^{N} R_{ij}\phi_\alpha(\mathbf{r}_j) = \lambda_\alpha \phi_\alpha(\mathbf{r}_j), \qquad i = 1, 2, \cdots, N. \tag{7}$$

The eigenvectors ϕ_1, ϕ_2, $\cdots$, ϕ_N are called Empirical Orthogonal Functions. Each ϕ_α is a 5 733-point $(21 \times 21 \times 13)$ distribution of non-seasonal temperature anomaly pattern. The eigenvalues, λ_α $(\alpha = 1, 2, \cdots, N)$, are all positive and the summation of them, $\sum\lambda_\alpha$, e-

quals the total variance. Therefore, λ_α is considered as the portion of total variance "explained" by the EOF ϕ_α. It is convenient to label the eigenfunctions ϕ_α so that the eigenvalues are in descending order, i, e.,

$$\lambda_1 > \lambda_2 > \lambda_3 > \cdots \tag{8}$$

The data matrix $\hat{T}$ $(\mathbf{r}_n, \bar{t}_p)$ becomes

$$\hat{T}(x_i, y_j, z_k, \tau_l, t_m) = \sum_\alpha PC_\alpha(\tau_l, t_m)\phi_\alpha(x_i, y_j, z_k), \tag{9}$$

where PC_α (τ_l, t_m) is the principal component representing the temporal variation of the associated spatial pattern described by the EOF mode, $\phi_\alpha(x_i, y_j, z_k)$.

Principal EOF modes

The first six leading EOF modes are able to account for 64.1% of the total variance (Table 2). The first two leading modes, EOF1 and EOF2, explain 44.4% of the total variance. Each EOF mode is three-dimensional and normalized so that its total spatial variance is equal to unity. We may easily see the vertically coherent structure of each mode.

Table 2. Variances of the first six leading temperature EOFs

EOF	Variance	Acumulative variance
1	0.267	0.267
2	0.177	0.444
3	0.071	0.515
4	0.059	0.574
5	0.037	0.611
6	0.030	0.641

The EOF1 mode.

The EOF1 mode (ϕ_1) shows frontal and multi-eddy structures. The frontal structure is evident in the northern SCS. Only positive values occur in the upper layer (above 75 m in depth) and both positive and negative values appear at the other depths (see Fig.13). However, we cannot use these positive/negative values of 1 to identify the warm of cool anomaly of the individual eddy. This is because the temperature anomaly, due to the EOF1 pattern, is the product of PC_1 and ϕ_1.

a. Western boundary current and frontal structures. From the surface to 30 m in depth, a bi-frontal structure (northeast-to-southwest oriented isolines) is the major thermal feature in the northern SCS (north of 12°N): a strong coastal front along the China coast, and a relatively weak and wide front across the SCS basin from the Vietnam coast to the Luzon island between 12°~17°N. The two fronts change their strengths synchronously, since the values of ϕ_1 are positive for the two fronts. The bi-frontal structure weakens with the depth and disappears at 50 m in depth. The front reoccurs from 75 m in depth and continues to be seen down to 300 m in depth. Below 75 m in depth in the northern SCS, ϕ_1 shows a northeast-tosouthwest orientedsingle front structure aligning to the China coast. The values of ϕ_1 across

the front change signs from negative near the China coast to positive in the middle of the northern SCS, indicating the out-of-phase variability of the front near the China coast and the deep basin.

Furthermore, we may notice that the values of ϕ_1 change signs from the top layer (0～30 m) to the lower layer (100～300 m) near the western boundary. This implies a strong baroclinicity of the western boundary currents with the opposite directions at the top layer and the lower layer.

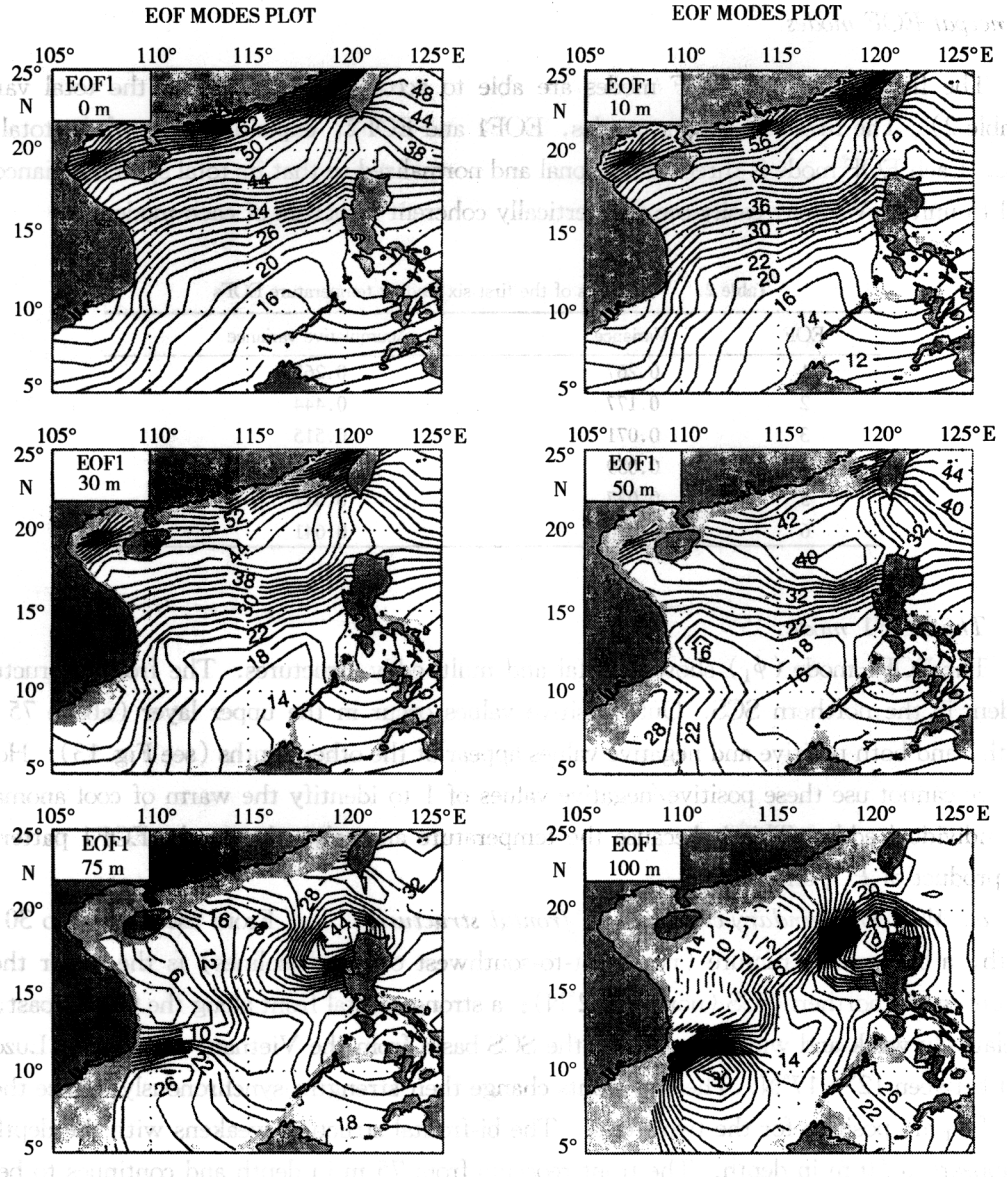

Fig. 13

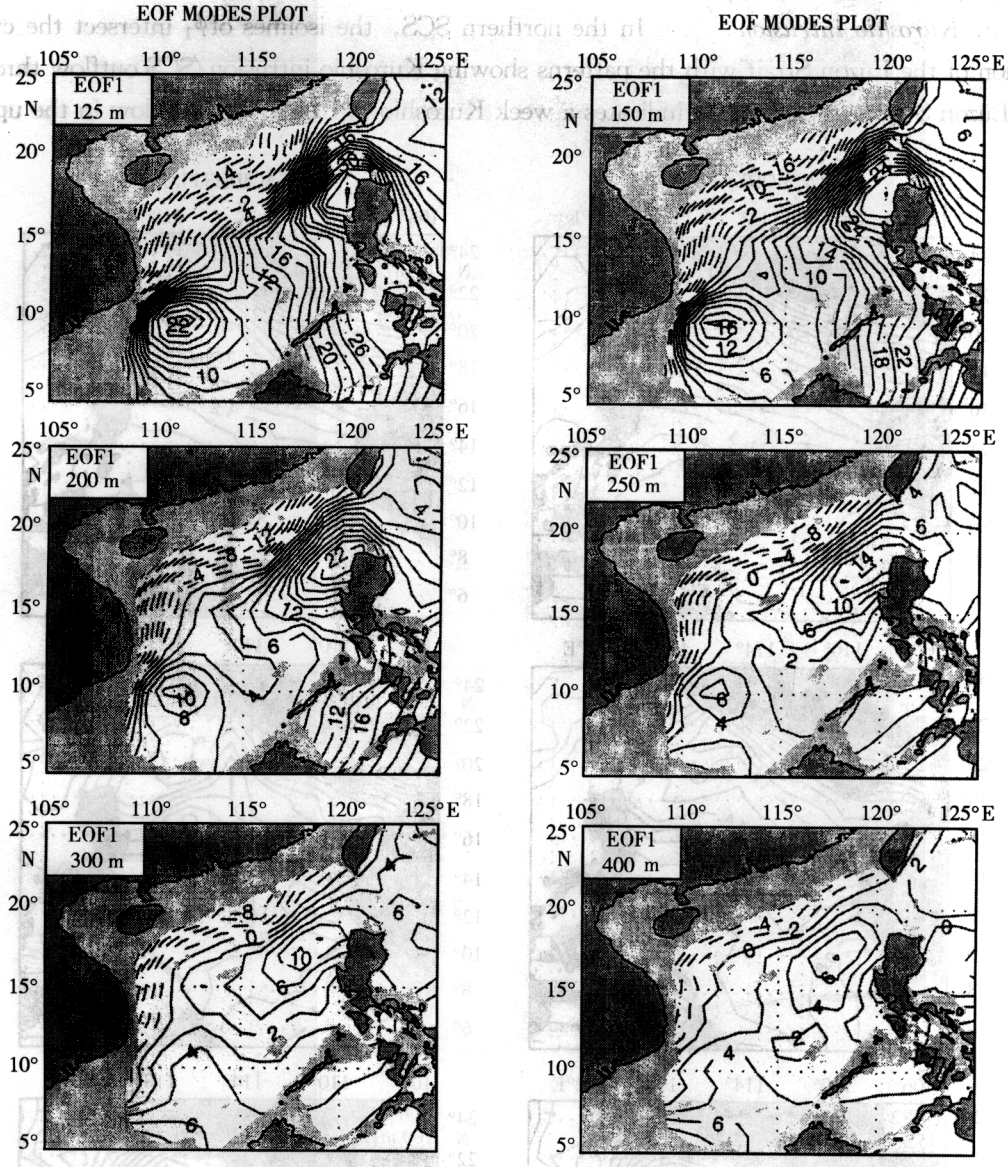

Fig. 13. EOF1 temperature anomalies (unit: 0.01℃).

b. Southern SCS multi-eddy structure. In the southern SCS (south of 12°N) from the surface to 30 m in depth, the EOF1 shows a dipole structure (dual eddies) with a high center (0.3℃) near the mouth of the Mekong River, and a low center (<0.14℃) in the west of the Borneo－Palawan Islands (WBP). This dipole structure is still quite evident from 30 m to 75 m in depth. Below 75 m in depth, the western eddy, near the Mokong River mouth, is much stronger than the eastern eddy. At 50 m in depth, an eddy (>0.4℃) appears in the northeastern SCS. This eddy slants towards the east (the Luzon Strait) with depth and becomes very strong in the layers between 75 m and 150 m. Below 150 m in depth,

this eddy reduces its strength.

c. Kuroshio intrusion. In the northern SCS, the isolines of ϕ_1 intersect the cross-section of the Luzon Strait with the patterns showing Kuroshio intrusion/SCS outflow through the Luzon Strait. This pattern indicates a week Kuroshio intrusion/SCS outflow in the upper

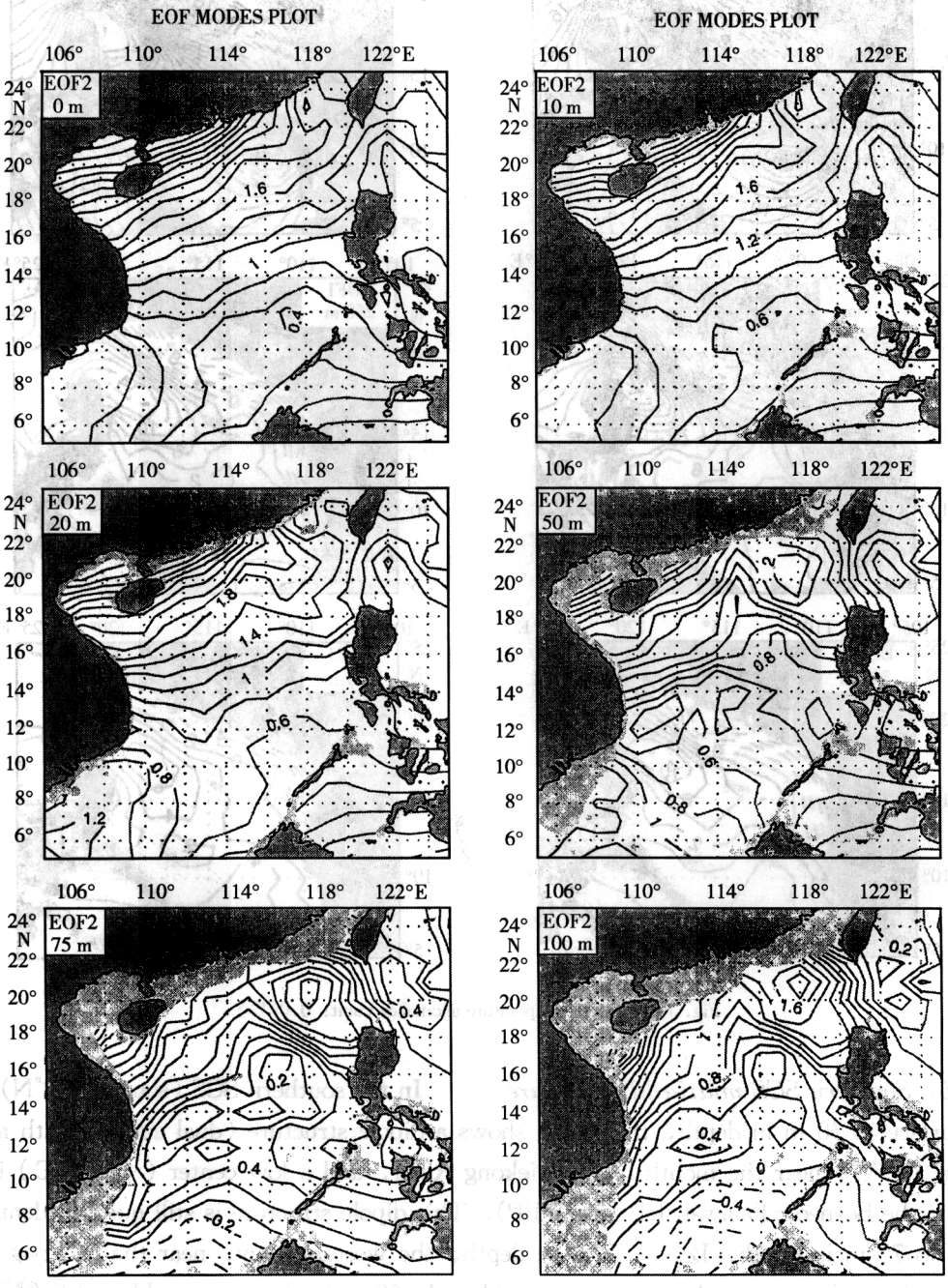

Fig. 14

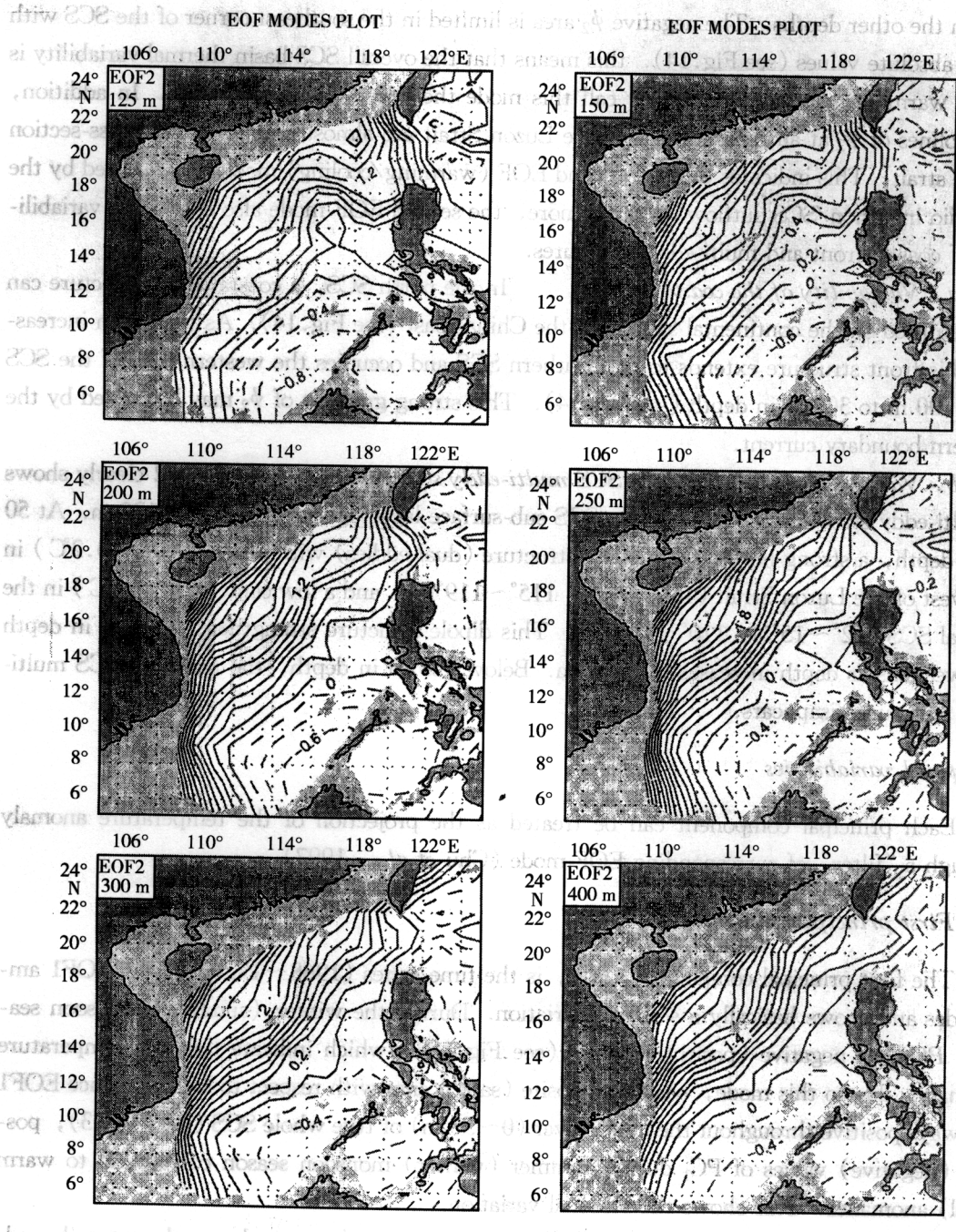

Fig. 14. EOF2 temperature anomalies (unit: 0.1℃).

layer above 50 m in depth, becoming stronger below 50 m in depth and reaching maximum strength in the layer between 100 m and 150 m in depth.

The EOF2 mode.

Similar to the first EOF mode, the second EOF mode (ϕ_2) has only positive values in the

upper layer from the surface to 50 m in depth and has both positive and negative values appearing on the other depths. The negative ϕ_2 area is limited in the southeast corner of the SCS with small absolute values (see Fig.14). this means that the overall SCS basin thermal variability is either warming or cooling. We may call this mode the warming/cooling mode. In addition, the isolines of ϕ_2 at all the depths near the Luzon Strait are almost parallel to the cross-section of the strait. This indicates that the second EOF (warming/cooling) mode is not caused by the Kurshio intrusion/SCS outflow. Furthermore, the second EOF mode also shows the variabilities of coastal front and multi-eddy structures.

a. Variability of the coastal front. In the north SCS, a coastal front structure can be identified on the continental shelf near the China coast (see Fig.14). As the depth increases, this front structure extends to the southern SCS and occupies the western part of the SCS from 100 m to 300 m in depth (see Fig.14). This strong gradient of ϕ_2 may be caused by the western boundary current.

b. Variability of the northern SCS multi-eddy structure. The EOF2 clearly shows a multi-eddy structure in the northern SCS sub-surface layer between 50 m and 125 m. At 50 m in depth, a strong north-south dipole structure (dual eddies) with a high center (0.2℃) in the west of the Luzon Strait (18°~22°N, 115°~119°E), and a low center (<0.04℃) in the central SCS (12°~15°N, 110°~116°E). This dipole structure strengthens at 75 m in depth and weakens as depth increases from 75 m. Below 125 m in depth, the northern SCS multi-eddy structure disappears.

Temporal variabilities

Each principal component can be treated as the projection of the temperature anomaly through a "filter" of corresponding EOF mode (Chu *et al*., 1997).

First principal component.

The first principal component, PC_1, is the time series (1968~1984) of the EOF1 amplitudes and shows basically a seasonal variation. During the winter (summer) monsoon season, PC_1 has negative (positive) values (see Fig.15), which indicate that the temperature anomaly, due to this mode, has the opposite (same) sign with respect to EOF1. Since EOF1 is always positive throughout the upper layer (0~50 m) of tthe whole SCS (see Fig.13), positive (negative) values of PC_1 during summer (winter) monsoon season correspond to warm (cool) anomalies. This shows the seasonal variation.

An interesting feature of the first EOF1 is its negative value near the northwestern boundary in the sub-surface layer (100~400 m). Since PC_1 has negative (positive) values during winter (summer) monsoon season, the thermal variability of the western boundary is out-of-phase with respect to the seasonal variabilith, that is , warm (cool) anomaly in the winter (summer) monsoon season.

Accordingly, the seasonal variation represented by PC_1 is not purely sinusoidal. The

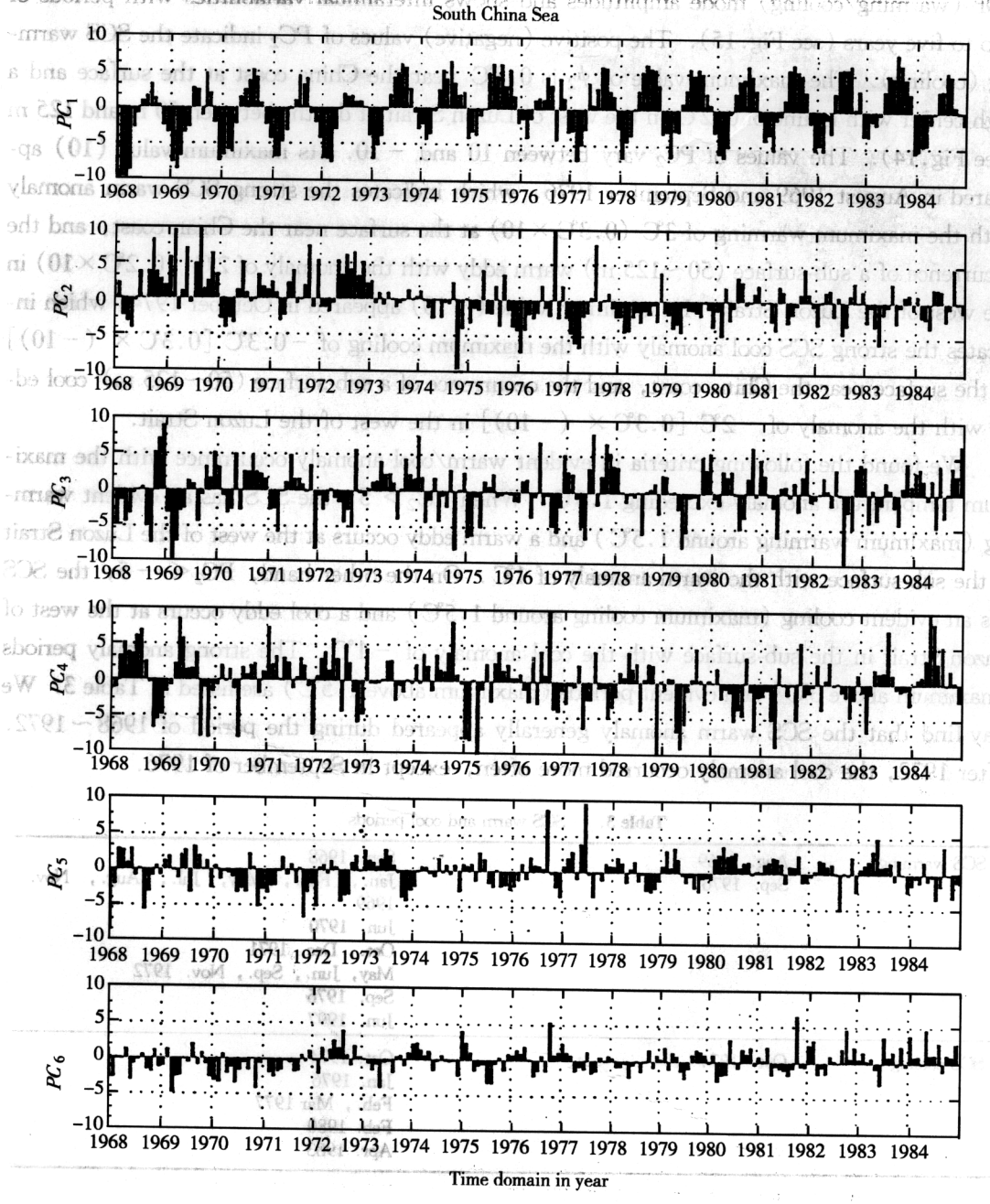

Fig. 15. The first six principal components for 1968～1984.

summer had a larger variability in the 1980's than in the early 1970's. However, the winter had a larger variability during 1968～1972 than the rest of the periods.

Second principal component.

The second principal component, PC_2, is the time series (1968～1984) of the second

EOF (warming/cooling) mode amplitudes and shows interannual variabilities with periods of two to five years (see Fig.15). The positive (negative) values of PC_2 indicate the SCS warming (cooling). The maximum value of ϕ_2 is 0.3℃ near the China coast at the surface and a high center with isoline of 0.2℃ in the west of Luzon Strait at depths between 50 m and 125 m (see Fig.14). The values of PC_2 vary between 10 and −10. Its maximum value (10) appeared in August 1969 and September 1976, which indicates the strong SCS warm anomaly with the maximum warming of 3℃ (0.3℃ × 10) at the surface near the Chian coast, and the occurrence of a sub-surface (50～125 m) warm eddy with the anomaly of 2℃ (0.2℃ × 10) in the west of the Luzon Strait. Its minimum value (−10) appeared in October 1974, which indicates the strong SCS cool anomaly with the maximum cooling of −0.3℃ [0.3℃ × (−10)] at the surface near the China coast, and the occurrence of a sub-surface (50～125 m) cool eddy with the anomaly of −2℃ [0.3℃ × (−10)] in the west of the Luzon Strait.

We found the following criteria in evident warm/cool anomaly occurrence with the maximum temperature anomaly exceeding 1.5℃. When $PC_2 > 5$, the SCS has an evident warming (maximum warming around 1.5℃) and a warm eddy occurs at the west of the Luzon Strait in the sub-surface with the warm anomaly of 1℃. On the other hand, $PC_2 < -5$, the SCS has an evident cooling (maximum cooling around 1.5℃) and a cool eddy occurs at the west of Luzon Strait in the sub-surface with the cool anomaly of −1℃. The strong anomaly periods (maximum above 3℃) and evident periods (maximum above 1.5℃) are listed in Table 3. We may find that the SCS warm anomaly generally appeared during the period of 1968～1972. After 1972, the cool anomaly occurred more often, except in September of 1976.

Table 3. SCS warm and cool periods

SCS warming	Aug. 1969 Sep. 1976	Sep. 1968 Jan., Feb., May, Jul., Aug., Nov. 1969 Jun. 1970 Oct., Dec. 1971 May, Jun., Sep., Nov. 1972 Sep. 1976 Jun. 1997
SCS cooling	Oct. 1974	Oct. 1974 Jan. 1976 Feb., Mar 1977 Feb. 1980 Apr. 1983

SEASONAL VARIATION OF SCS CIRCULATION

We use a recently developed P − vector inverse method (Chu, 1995, Chu *et al*., 1998 a, b) to compute the absolute geostrophic velocity from monthly mean T, S fields. Chu *et al*. (1998b) shows the advantages of using the P − vector method, namely, the easy identification of the two necessary conditions for β-spiral inverse method: (1) intersection between the isopycnal and iso-potential vorticity surfaces (existence of the vector P), and (2) the turning

(turning of the vector P). For water columns satisfying the two necessary conditions, we may use the P – vector method to obtain absolute geostrophic velocity. For further details and validation of the algorithm presented, see Chu *et al*. (1998a).

General description

The most obvious of the inverted summer and winter SCS circulation are flow separation, basin gyres, and mesoscale eddies. Hinted in Wyrtki's (1961) depiction but more explicit in our computation, are the upper level (10 m depth) west-to east cross-basin currents, which are almost parallel to 16°N latitude from February to July. The inverted monthly SCS circulation agrees quite well with earlier observational study (Wyrtki, 1961). As the commonly used inverse methods, the P – vector-inverted western boundary currents are somewhat small. This could be caused by the neglect of relative vorticity in the potential vorticity calcuation (Chu, 1995).

Surface circulation

During the winter monsoon period (November to March), the winter Asian high pressure system brings strong winds from the northeast, and the SCS surface circulation pattern is cyclonic (Wyrtki, 1961). At the surface inflow from the Luzon Strait (the Kuroshio intrusion) turns southwest along the Asian continental shelf, then south along the coast of Vietnam (see Fig.16). In November, this current splits into two currents at 12°N: a southward alongshore current and an eastward off-shore current. The southward branch turns east at 6°N, then turns northeast and joins the eastern branch at 115°E. An evident multi-eddy structure is obtained with two cyclonic eddies in the north SCS (north of 12°N) and cyclonic and anticyclonic eddies in the southern SCS (south of 12°N). The eddy near Luzon was first identified by Nitani (1970) from the surface data. We may call it Luzon cyclnic eddy. The flow pattern does not change vary much from November to December, except that the cyclonic eddy near the Luzon Strait strengths. It should be noticed that the anticyclonic circulation between SCS and the Sulu Sea around Palawan Islands might not be realistic.

In January, the west cyclonic eddy in the northern SCS expands toward the south. In March, the west cyclonic eddy in the northern SCS disappears and instead a cross-basin flow appears along 16°N latitude and joins the cyclonic eddy near the Luzon Strait. The southern SCS is occupied by an anticyclonic eddy. This anticyclonic eddy expands to the north and forms the only evident eddy in the central SCS in March (see Fig.16). This eddy is associated with the central SCS warm pool in spring (see Fig.16) and expands toward the south in April. May is the month of the summer monsoon transition. The anticyclonic eddy reduces its strength and becomes unidentifiable.

During the summer monsoon period (June to September), winds blow from the southwest and the SCS surface circulation generally follows suit with anticyclonicity in the southern basin (Wyrtki, 1961). Inflow is through the southern boundary and outflow is through the north-

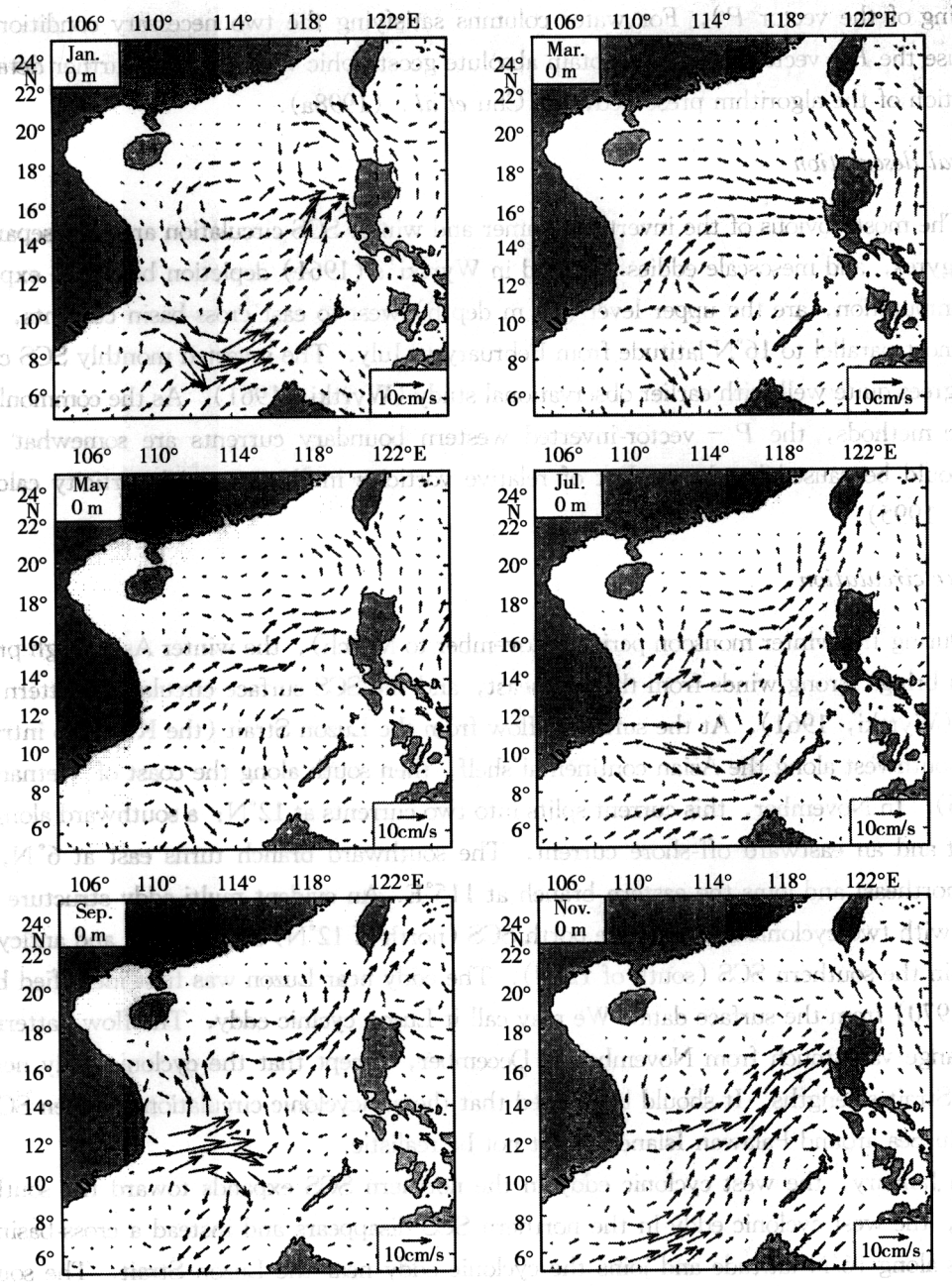

Fig. 16. Inverted monthly mean surface circulation: January, March, May, July, September and November.

ern Taiwan Strait and eastern Luzon Strait. The inverted July menas that the general circulation pattern has the following features. Velocities reach 20 cm/s near the Vietnam coast and split into two currents at 12°N: the coastal current and off-shore current. The off-shore current further bifurcates and partially leaves the coast; the bifurcation point is at 110°E. The northern branch moves northeast to 113°E and then turns zonally between 15°～18°N. The

southern branch moves zonally until reaching Palavan Island, then turns north and joins with the north branch at 16°N. A cyclonic eddy appears in July near the south Vietnam coast and strengthens in August. This eddy was reported by Dale (1956) and Uda and Nakao (1974).

Sub-surface (75 m)

The sub - surface (75 m) shows a strong seasonal variation (Fig. 17). Warm and salty

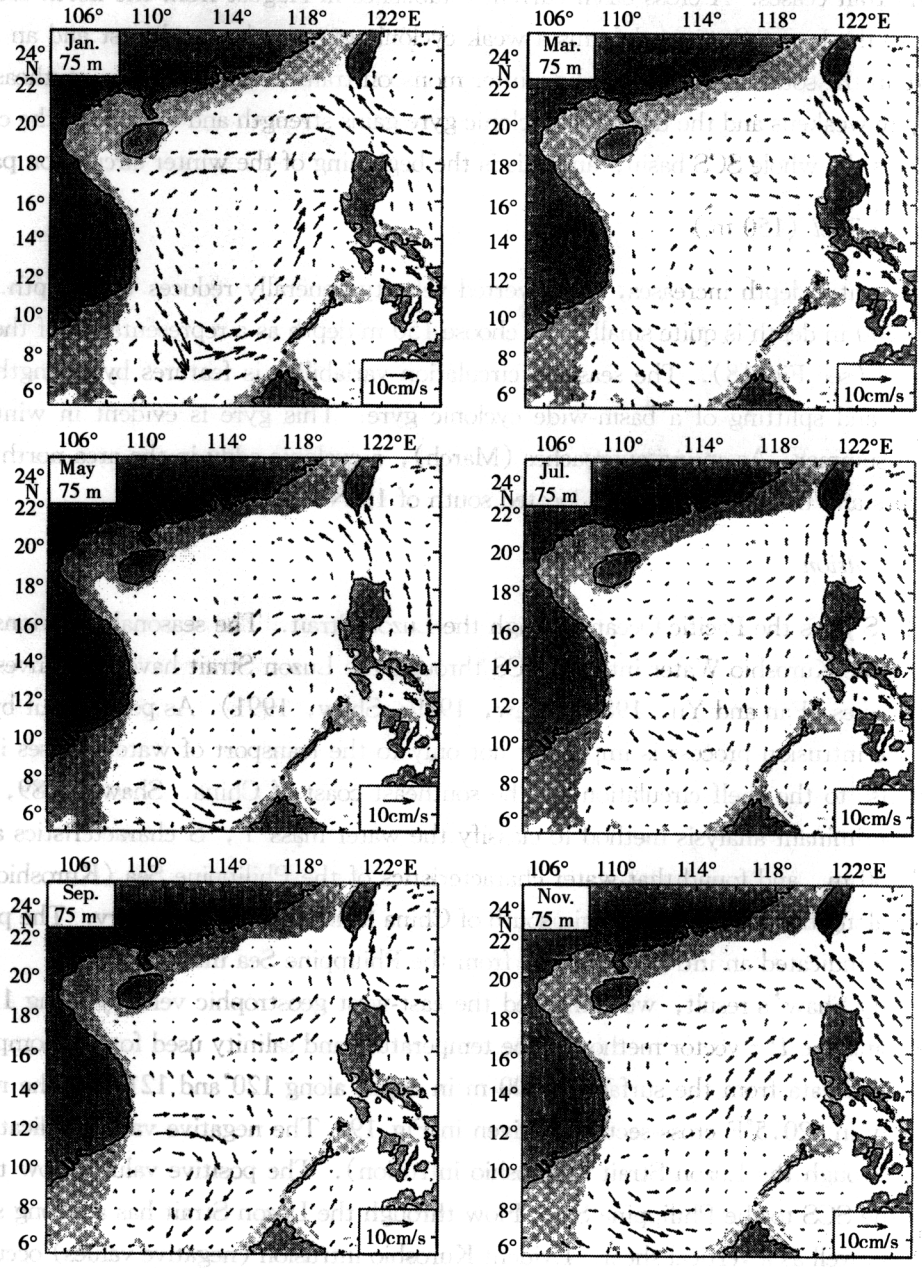

Fig. 17. Inverted monthly mean sub-surface (75 m) circulation: January, March, May, July, September and November.

Kuroshio water enters the SCS through the Luzon Strait in October – March, the transition to and during the winter monsoon season. The winter circulation pattern is the basin-wide cyclonic gyre. A cyclonic mesoscale eddy splits from the gyre near the Luzon Strait in January and keeps its strength in February. On the other hand, the basin-wide cyclonic gyer weakens and shrinks toward the southwest in February and disappears in March.

During the summer monsoon period (June – September), the Kuroshio intrusion through the Luzon Strait ceases. A cross-basin current establishes in August from the north branch of that eddy to the Luzon Strait and forms a weak cyclonic gyre in the northwest and an anticyclonic gyre in the southeast. During the winter monsoon transition period, the southeast anticyclonic gyre weakens and the northeast cyclonic gyre gains strength and eventually the cyclonic gyre occupies the whole SCS basin, and this is the beginning of the winter circulation pattern.

Intermediate level (150 m)

As the water depth increases, the inverted velocity generally reduces with depth. 0The velocity at 200 m depth is quite small. We choose 150 m depth as a representative of the intermediate level (see Fig.18). The seasonal circulation variability is features by strengthening, weakening, and splitting of a basin-wide cyclonic gyre. This gyre is evident in winter and weakens in summer. As spring approaches (March), a cyclonic eddy in the area northwest of Luzon occurs and the cyclonic gyre is located south of 16°N.

Kuroshio intrusion

The SCS joins the Pacific Ocean through the Luzon Strait. The seasonal variations of the intrusion of the Kuroshio Water into the SCS through the Luzon Strait have been investigated in earlier studies (Fan and Yu, 1981; Shaw, 1989; Shaw, 1991). As pointed out by Shaw (1991), the intrusion process is important not only to the transport of water masses into the SCS, but also to the shelf circulation off the southeast coast of China. Shaw (1989, 1991) used the discriminant analysis method to classify the water mass T, S characteristics at 150, 200, and 250 m, and found that water characteristics of the Philippine Sea (Kuroshio) were identifiable along the continental margin south of China from October to January. The presence of this water indicated an intrusion current from the Philippine Sea into the SCS.

To verify Shaw's result, we computed the east-west geostrophic velocity along 120.5°E longitude using the P – vector method. The temperature and salinity used for the computation are the gridded data from the surface to 400 m in depth along 120°and 121°E. The monthly zonal velocity in 120.5°E cross-section is given in Fig.19. The negative values indicate westward flow through the Luzon Strait (Kuroshio intrusion). The positive values show the outflow from the SCS to the Philippine Sea. Flow through the Luzon Strait has a strong seasonal variation, as well as a vertical shear. Evident Kuroshio intrusion (negative values) occurs during the winter monsoon season (November – March) in the upper 200 m. Below 200 m, the velocity is quite small, and most values are positive. The computed upper layer (0 ~ 400 m)

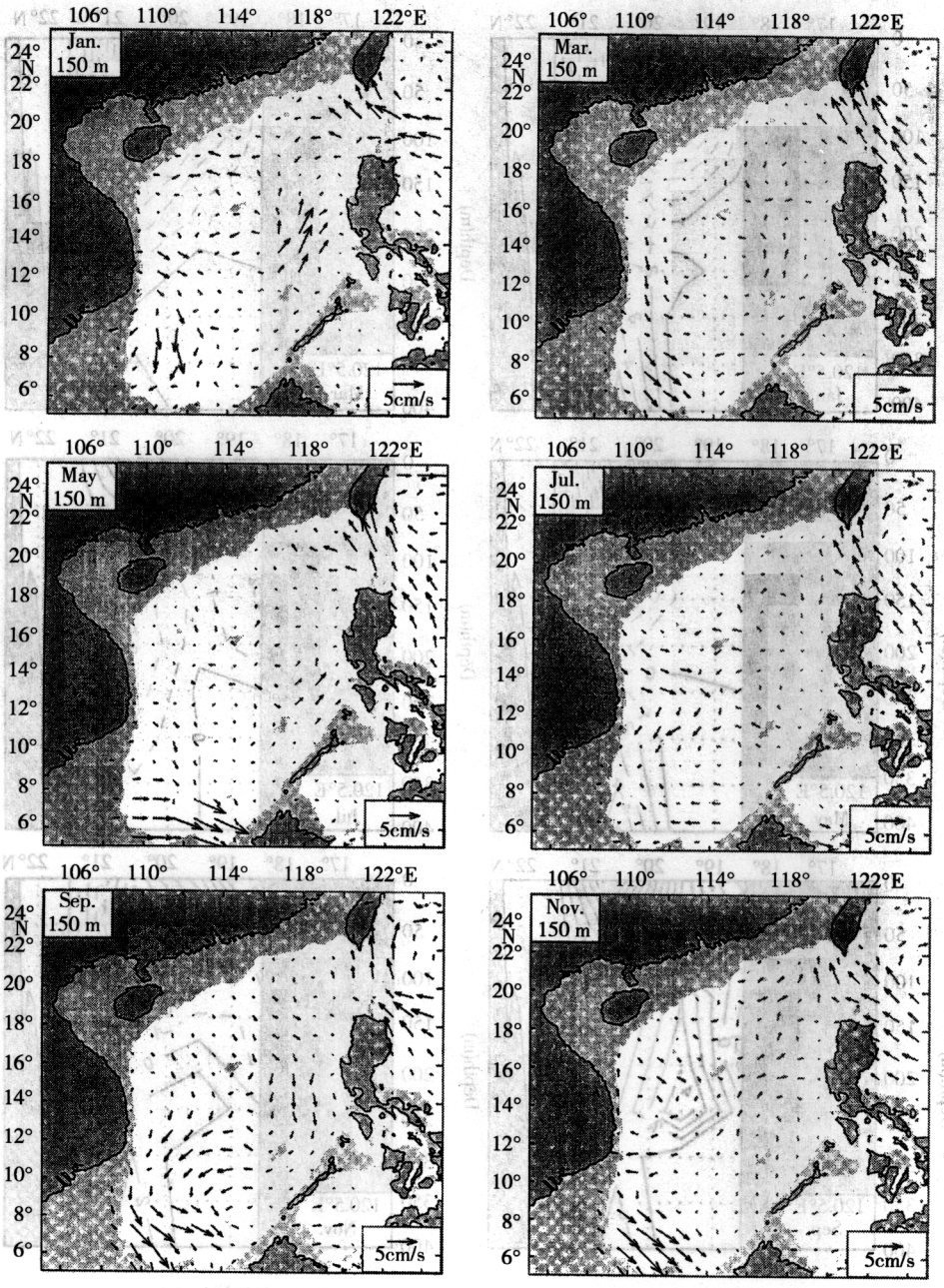

Fig. 18. Inverted monthly mean intermediate level (150 m) circulation: January, March, May, July, September and November.

volume transport through the Luzon Strait has a strong seasonal variation: the maximum Kuroshio intrusion into the SCS with a value of -2.2 Sv ($1\ \text{Sv} = 10^6 \text{m}^3 \cdot \text{s}^{-1}$) occurring in March, and the maximum SCS outflow with a value of 1.5 SV in September. These values are consistent with Wyrtki's (1961) estimation.

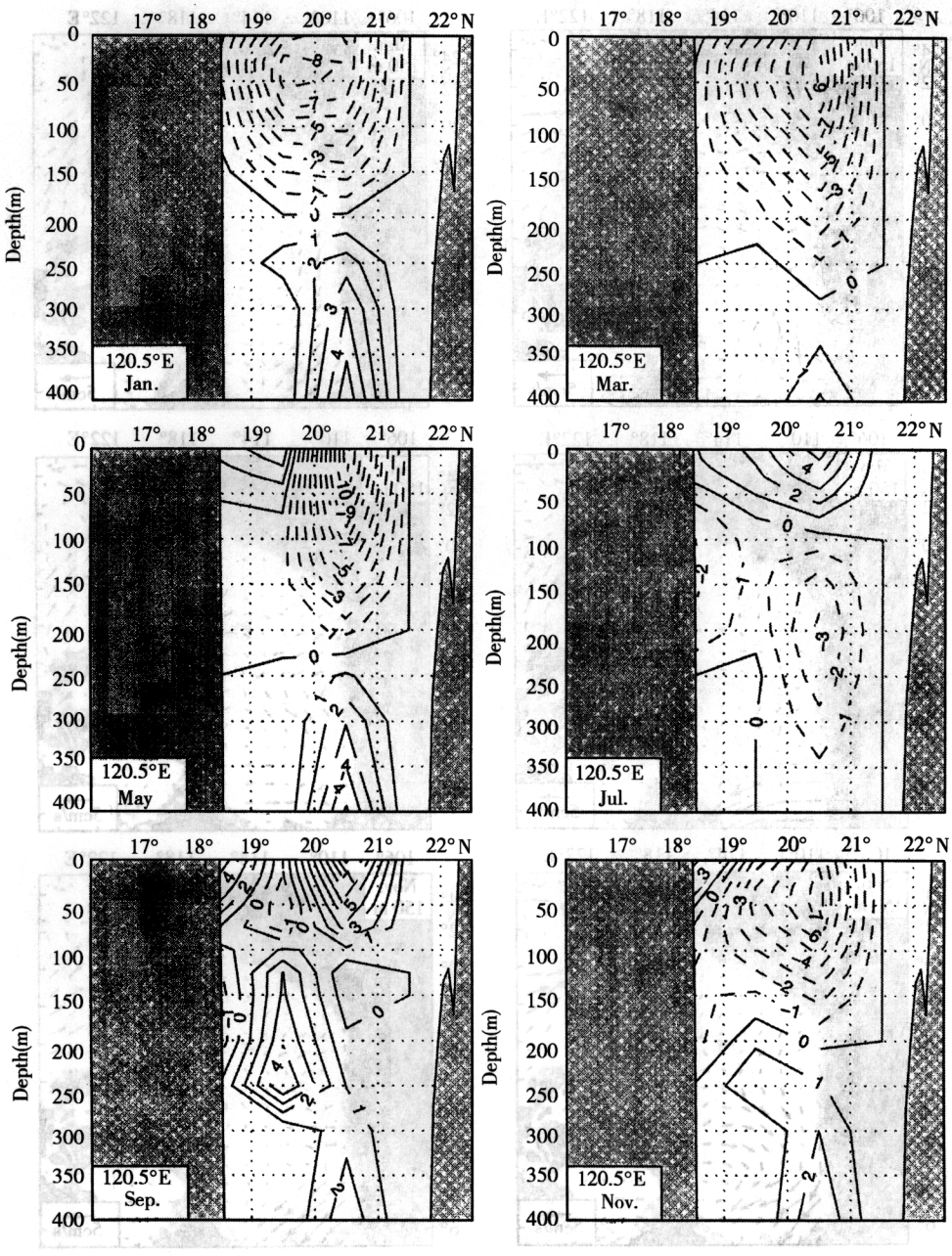

Fig. 19. Inverted monthly mean zonal velocity at Luzon Strait (120°E): January, March, May, July, September and November.

CONCLUSIONS

The goal of this study is to investigate the thermohaline structure and the circulation patterns of the South China Sea using the historical MOODS hydrographic data. We applied the minimum curvature with spine method to produce thirteen level gridded data from the MOODS. Although the MOODS contain more than 180 000 temperature profiles, the deeper

layer (below 400 m in depth) is poorly sampled. Furthermore, the MOODS contain only 14 000 salinity profiles, so we were only able to establish climatological annual and monthly mean salinity fields at thirteen levels above 400 m in depth. After the establishment of the gridded temperature and salinity data, we used the composite and EOF analysis to get the seasonal and interannual variabilities of the SCS thermohaline structure, and the P - vector inverse method to obtain the three-dimensional absolute geostrophic velocity fields. The major results from this research are summarized as follows.

(1) The annual mean (1968~1984) temperature $\bar{\bar{T}}$ field over the SCS shows the pattern of northeast-southwest oriented isotherms at the upper layer from the surface to 20 m depth with a weak gradient from 28.5℃ near the Borneo coast to 25℃ near the southeast China coast. A strong temperature front is found near the Luzon Strait in the sub-surface layer from 100 m to 400 m. The SCS water temperature is quite uniform (e. g., near 13℃ at 250 m) and much lower than the water east of the Luzon Strait, the West Pacific Ocean Water. The annual mean salinity $\bar{\bar{S}}$ shows that in the upper layer, a large amounts of freshwater enter the SCS from the Zhujiang River in the northwest and from the Mekong River in the southwest. The Kuroshio brings the high salinity water through the Luzon Strait into the north SCS and forms a salty tongue (34 psu) stretching into the Southeast China coast.

(2) Seasonal thermohaline variability is associated with fronts and multi-eddies. The bi-frontal structure is the major thermal feature in the northern SCS (north of 12°N): a strong coastal front along the China coast, and a relatively weak and wide front across the SCS basin from the Vietnam coast to the Luzon Island between 12°~17°N. The two fronts change their strengths synchronously; they weaken with the depth and disappear at 50 m in depth. The front reoccurs from 75 m in depth and is evident as deep as 300 m in depth. At 30 m in depth, an eddy (>0.4℃) appears in the northern SCS and slants toward the east (the Luzon Strait) with depth and becomes very strong in the layer between 75 m and 150 m. Below 150 m in depth, this eddy reduces its strength. In the southern SCS (south of 12°N) from the surface to 30 m in depth, a dipole structure (dual eddies) was found with a warm (cool) eddy near the Mekong River mouth, and a cool (warm) eddy in the west of the Borneo - Palawan Islands during the summer (winter) monsoon season. Below 75 m in depth, the western eddy near the Mekong River mouth is much stronger than the eastern eddy. The seasonal salinity variability was also identified. During winter (January), a salty tongue 1.2 psu anomaly stretches from the Luzon Strait to the continental shelf along the Southeast China coast, representing a strong Kuroshio intrusion. A weak fresh anomaly (-0.2 psu) is found in the west of Luzon Island. During the summer (July), a salty tongue with 0.4 psu stretches from the Vietnam coast to 118°E between 10°~17°N, occupying the central SCS while the rest is occupied by negative anomaly. A strong fresh tongue occupies the continental shelf along the Southeast China coast and the Gulf of Tonkin.

(3) Both water mass analysis and the inverted geostrophic velocity at the Luzon Strait confirm the Kuroshio intrusion during the winter monsoon season. Such an intrusion has a vertical

shear. Evident Kuroshio intrusion (negative values) occurs during the winter monsoon season (November－March) in the upper 200 m while below 200 m the velocity is quite small and outflows from the SCS into the Philippine Sea. The computed upper layer (0～400 m) volume transport through the Luzon Strait has a strong seasonal variation: the maximum Kuroshio intrusion into the SCS with a value of －2.2 Sv occurring in March, and the maximum SCS outflow with a value of 1.5 Sv in September.

(4) The interannual SCS warming/cooling phases were identified by the second EOF mode with periods of two to five years. The strongest SCS warming occurred in August 1969 and September 1976, with a warming of 3℃ at the surface near the China coast and an occurrence of a sub-surface (50～125 m) warm eddy (2℃) in the west of Luzon Strait. The strongest SCS cooling appeared in October 1974 with a coolng of 3℃ at the surface near the China coast, and an occurrence of a sub-surface (50～125 m) cool eddy (－2℃) in the west of the Luzon Strait. The warming events appeared between the late 1960's and first half of the 1970's, and the cooling events occurred in the second half of the 1970's and early 1980's.

(5) The T, S and the inverted velocity fields show the multi-eddy structure: two cyclonic eddies in the north SCS (north of 12°N) and cyclonic and anticyclonic eddies in the southern SCS (south of 12°N). The anticyclonic warm-core eddy expands to the north and forms the only evident eddy in the central SCS in March, and expands toward the south in April. May is the month of the summer monsoon transition. The anticyclonic warm-core eddy reduces its strength and becomes unidentfiable. During the summer monsoon period (mid-May to August), winds blow from the southwest and the SCS surface circulation generally follows suit with anticyclonicity in the southern basin. Inflow is through the southern boundary and outflow is through the northern Taiwan Strait and eastern Luzon Strait. The inverted July mean general circulation pattern shows that velocities reach 20 cm/s near the Vietnam Coast and splits into two currents at 12°N: the coastal current and off-shore current.

REFERENCES

Cheang B. K. (1980) Some aspects of winter monsoon and its characteristics in Malaysia. *Res. Publ.*, Maylaysian Meteorological Service, Kuala Lumpur, No. 2.

Chu P. C. (1995) P－vector method for determining abosolute velocity from hydrographic data. *Mar. Technol. Soc. J.*, **29**(3), 3～14.

Chu P., C. Chang (1997) South China Sea warm Pool in boreal spring. *Adv Atmos. Sci.*, **14**, 195～206.

Chu P. C., H. C. Tseng, C. P. Chang, J. M. Chen (1997a) South China Sea warm pool detected in spring from the Navy's Master Oceanographic Observational Data Set (MOODS). *J. Geophys. Res.*, **102**, 15761～15771.

Chu P. C., S. H. Lu, Y. C. Chen (1997b) Temporal and spatial variabilities of the South China Sea surface temperaure anomaly. *J. Geophys. Res.*, **102**, 20 937～20 955.

Chu P. C., S. K. Wells, S. D. Haeger, C. Szczechowski, M. Carron (1997c) Temporal and spatial scales of the Yellow Sea thermal variability. *J. Geophys. Res.*, **102**, 5 655～5 667.

Chu P. C., C. W. Fan, W. J. Cai (1998a) Evaluation of P－vector method using modular ocean model (MOM). *J. Oceanogr.*, **54**, 185～198.

Chu P. C., C. W. Fan, C. J. Lozano, J. L. Kirling (1998b) An airborne expandable bathythermograph survey of the South China Sea, May 1995. *J. Geophys. Res.*, **103**, 21 637~21 652.

Chu P. C., C. W. Fan (2001) Low salinity cool-core cyclonic eddy detected northwest of Luzon during the South China Sea monsoon experiment (SCSMEX) in July 1998. *J. Oceanogr.*, **57**, 549~563.

Dale W. L. (1956) Winds and drift currents in the South China Sea. *Malayan J. Trop. Geogr.*, **8**, 1~31.

Gandin L. S. (1965) Objective analysis of meteorological fields. *Israel Program for Scientific Translation, Jerusalem*, 242 pp.

He Y., C. Guan, H. Gao (1996) Water temperature and circulation structure in the upper ocean of the northern South China Sea. *Oceanography in China* (in Chinese with English abstract), China Ocean Press, Beijing, **6**, pp. 60~69.

Huang Q. Z., W. Z. Wang, Y. S. Li, C. W. Li (1994) Current characteristics of the South China Sea. *Oceanology of China Seas*, edited by D. Zhou, Y. B. Liang, and C. K. Tseng, Kluwer Acad., Norwell, Mass.

Lozano C. J., A. R. Robinson, H. G. Arango, A. Gangopadhyay, Q. Sloan, P. J. Haley, L. Anderson, W. Leslie (1996) An interdisciplinary ocean prediction system: assimilation strategies and structure data model. *Modern Approaches to Data Assimilation in Ocean Modeling*, edited by P. Malanotte-Rizzoli, Elsevier, Amsterdam, pp. 413~452.

Ma B. B. (1998) The South China Sea thermohaline structure and circulation. *Master Thesis*, Naval postgratuate School, Monterey, California, pp. 254.

Nitani H. (1970) Oceanographic conditions in the sea east of Philippines and Luzon Strait in summer of 1965 and 1966. *The Kuroshio – A Symposium on Japan Current*, edited by J. D. Marr, East-West Press, Honolulu, Hawaii, pp. 213~232.

Soong Y. S., J. H. Hu, C. R. Ho, P. P. Niiler (1995) Cold-core eddy detected in South China Sea. *EOS*, 345~347.

South China Sea Institute of Oceanology (SCSIO) (1985) *Integrated Investigation Report on Sea Area of the South China Sea* (in Chinese), Science Press, Beijing, **2**, pp.183~231.

Uda M., T. Nakao (1972) Water masses and currents in the South China Sea and their seasonal changes. *Paper presented at the 3rd Cooperative Study of the Kuroshio and Adjacent Regions (CSK) Symposium*, UNESCO, Bangkok, Thailand.

Wang L., C. Koblinsky, S. Howden, N. Huang (1999) Interannual variability in the South China Sea from expandable bathythermograph data. *J. Geophys. Res.*, **104**, 23 509~23 523.

Wyrtki K. (1961) Scientific results of marine investigations of the South China Sea and Gulf of Thailand 1959~1961, *Naga Rep.*, 2, Scripps Institution of Oceanography, University of California, San Diego, pp. 164~169.